North Atlantic Oscillation polarity during the past 3000 years ~~ka~~ derived from ~~lacustrine~~ sediments of large lowland lake Schweriner See, NE-Germany

Marie-Luise Adolph[1*], Sambor Czerwiński[1,2,3], Mirko Dreßler[1], Paul Strobel[43], Marcel Bliedtner[34], Sebastian Lorenz[1], Maxime Debret[45], Torsten Haberzettl[1]

[1] Department of Physical Geography, Institute for Geography and Geology, University of Greifswald, Germany
[2] Climate Change Ecology Research Unit, Faculty of Geographical and Geological Sciences, Adam Mickiewicz University in Poznań, Poland
[3] Department of Geomorphology and Quaternary Geology, University of Gdańsk, 80-309 Gdańsk, Poland
[4] Department of Physical Geography, Institute for Geography, Friedrich-Schiller-University Jena, Germany
[54] UMR 6143 M2C Laboratoire Morphodynamique Continentale et Côtière, Department of Geoscience, Université de Rouen Normandie, France

Correspondence to: Marie-Luise Adolph (marie-luise.adolph@uni-greifswald.de)

Abstract

~~.~~ Based on a multi-dating and multi-proxy approach, we reconstruct Late Holocene environmental changes derived from sediments of Schweriner See, a large lowland lake in NE-Germany, ~~spanning~~covering the past $3070^{+170}/_{-210}$ cal BP. We infer ~~large-scale atmospheric~~ variations in large-scale atmospheric circulation systems ~~using~~from a combination of in-lake productivity indicators ~~using~~ derived from traditional and high-resolution techniques (e.g. LOI_{550}, TOC, ~~inc/coh~~inc/coh)~~,~~ diatom assemblages, ~~which are sensitive to ice-cover duration,~~ as well as compound-specific hydrogen isotopes ($\delta^2 H_{C25}$). Before 1850 CE, both ~~reflecting variability in the moisture source region distinguishing the southern and northern North Atlantic and/or Arctic region and/or the degree of evaporative lake water enrichment. Our study shows that before 1850 CE, in-lake productivity at Schweriner See was mainly influenced by winter temperature variability, which modulates ice-cover duration and growing-season length.~~ productivity and the occurrence or disappearance of the diatom species *S. chantaicus* reflect winter temperature variability, while variations in the compound-specific hydrogen isotopes suggest changes in the moisture source region. We observe distinct variation between i) milder winter temperatures with a moisture source region in the southern North Atlantic, and ii) colder winter temperatures with a moisture source in the northern North Atlantic and/or Arctic regions. Such distinct variations in winter temperatures and moisture source region sources are mainly modulated by the North Atlantic Oscillation (NAO), which affects i.a. Westerly strength and pathways and, eventually, winter temperature and moisture source region for northern Central Europe. Besides these long-term shifts in atmospheric conditions, short-term variations in titanium can be linked to shoreline distance, i.e. lake-level variability, likely influenced by changes in precipitation and/or evaporation, and after the 12th century to anthropogenic impacts. Since $105^{+95}/_{-75}$ cal BP, productivity has been driven by nutrient availability related to anthropogenic activities.

Low productivity co-occurs with the occurrence of the diatom species *Stephanocostis chantaicus*, which blooms below the ice cover, indicating temporal prolonged ice cover duration. Simultaneously, changes to a moisture source region in the northern North Atlantic and/or Arctic regions and/or low evaporative lake water enrichment are inferred from δ^2H_{C28}. In contrast, high productivity is linked to the disappearance of *S. chantaicus* and moisture originating from the southern North Atlantic and/or high evaporative lake water enrichment. These distinct changes are driven by variations between positive and negative NAO polarity during the past $3070^{+170}/_{-210}$ cal BP. Besides these long-term shifts in atmospheric conditions, short-term variations can be inferred from titanium concentrations, which mainly reflect paleo-shoreline distance likely linked to precipitation variability and, after the 12th century, to anthropogenic impacts. Since 1850 CE, productivity has been driven by nutrient availability related to anthropogenic activities.

1 Introduction

In recent decades, ~~hydroclimatic conditions in Central Europe have been characterized by~~ droughts ~~have~~ which have been increas~~ing~~ed in frequency and severity ~~in Central Europe~~ (Spinoni et al., 2018) and ~~and had~~resulting resulted in ~~with~~ severe socio-economic and ecological consequences. Future climate scenarios for Western and Central Europe predict increasing temperatures, more frequent, longer and/or more intense heat waves, as well as warm spells and an increase in dryness with short-term droughts (IPCC, 2021) affecting the hydrological cycle and, therefore, all aquatic (eco)systems. Some areas in Western and Central Europe, such as NE-Germany, have already been affected by l~~L~~owering lake and groundwater levels ~~in~~ ~~Central Europe, such as in Northeast Germany (Germer et al., 2010),~~Lowering lake and groundwater levels in Central Europe, ~~such as in Northeast Germany (Germer et al., 2010), has already affected some areas in Central Europe~~. However, to understand the drivers, magnitude and direction of climatic and environmental changes and to assess future developments, longer time series than those provided by monitoring efforts are needed (IPCC, 2021).

Late Holocene hydroclimatic variability in Western and Central Europe has been related to changes in ocean circulation (e.g. Trouet et al., 2012; Bond et al., 2001), solar cycles (e.g. Martin-Puertas et al., 2012; Mellström et al., 2015) and atmospheric circulation systems such as the North Atlantic Oscillation (NAO). The NAO is one of the leading atmospheric circulation systems influencing weather and climate conditions in the Northern Hemisphere (Bliedtner et al., 2023; Hurrell and Deser, 2009). It refers to changes in the atmospheric mass balance, i.e., the air pressure difference between the subpolar low (Iceland) and subtropic high (Azores) sea-level pressure (SLP) systems. These, in turn, influence surface air temperature, precipitation, wind and storminess, including wind direction and storm tracks (Hu et al., 2022). The NAO is more active in the cold season (October–April), with larger amplitudes and a strong influence on winter temperature and precipitation (Hurrell et al., 2003). The NAO index is defined as two modes depending on the barometric difference between the pressure systems: i) a positive NAO (NAO+) is associated with a stronger gradient between the pressure systems causing zonal circulation and increased intensity of cyclones, i.e. in stronger Westerlies (Hurrell and Deser, 2009) and generally mild and moist (maritime) winter conditions, and in contrast, ii) a negative NAO (NAO-) has a weaker gradient causing a meridional circulation with weaker Westerlies, which results in more frequent atmospheric blocking and allows colder air from the Arctic regions to flow towards Europe (Hurrell and Deser, 2009) and is generally associated with cold and dry (continental) winter conditions (Fig. 1A). Recently, it has been suggested that winter conditions in the North Atlantic region can be linked to the combined effects of the NAO and the second mode of variability, i.e. the Eastern Atlantic pattern (EA) (e.g. Comas-Bru and McDermott, 2014; Mellado-Cano et al., 2019). The EA pattern is defined as sea-level pressure monopole between Iceland and Ireland (e.g. Comas-Bru and McDermott, 2014; Moore et al., 2013) modulating the location and intensities of the Icelandic Low and Azores High (e.g. Moore et al., 2011) and consequently, e.g. the position of the North Atlantic storm tracks and jet stream (Woollings et al., 2010; Seierstad et al., 2007; Moore and Renfrew, 2012).

~~The r~~Recent climate in North Germany has a spatial climatic gradient with increasing continentality from west to east. ~~EE~~xisting paleoenvironmental studies from North Germany point to considerable environmental variability during the

Holocene (e.g. Dietze et al., 2016; Theuerkauf et al., 2022; Kaiser et al., 2012) but have rarely been linked to NAO variability (e.g. Zahrer et al., 2013) even though coastal areas surrounding the Baltic Sea were identified as ideal for collecting proxy information of large-scale North Atlantic atmospheric patterns (e.g. NAO) (Comas-Bru et al., 2016). So far, an in-depth understanding of the Holocene hydroclimatic variability of North Germany is still limited because the majority of studies have been carried out in areas affected by more continental climate (e.g. Dietze et al., 2016; Lampe et al., 2009; Lorenz, 2007; Theuerkauf et al., 2022). Studies from the transition from maritime to continental climate conditions are rare (e.g. Lorenz, 2007). Moreover, many studies have been carried out on small lacustrine systems (e.g. Dreßler et al., 2011), in which anthropogenic impact may overprint natural climate variations (Haberzettl et al., 2019). These biases culminate in sometimes contradicting results, e.g. in reconstructed lake-level curves, which have been used as key tools for hydroclimatic reconstructions so far (Kaiser et al., 2012). Apart from that, some studies from that area stress that not all observed lake-level variations are induced by climatic variations but rather by (anthropogenic) landcover changes influencing evapotranspiration and, consequently, groundwater recharge (e.g. Theuerkauf et al., 2022; Dietze et al., 2016).

In this study, we hypothesize that Schweriner See, a large hard-water lake located approximately 20 km south of the Baltic Sea and close to the boundary between more maritime to more continental climate, is a suitable archive to reconstruct the impacts of large-scale atmospheric circulation patterns on the North German lowlands. As Schweriner See is a rather large lake, we hypothesize that the lake is less susceptible to anthropogenic biases that may be experienced when investigating small lacustrine systems and reflects (supra)regional hydroclimatic variations. Moreover, Schweriner See has a relatively small catchment compared to its size (Wöbbecke et al., 2003), making it sensitive to hydrological changes.

~~and a spatial climatic gradient with increasing continentality from west to east, which is influenced by internal dynamics of the climate system such as the North Atlantic Oscillation (NAO) governing precipitation and surface air temperature (Hurrell, 2003). However, an in-depth understanding of the Holocene hydroclimatic variability of North Germany is still limited because the majority of studies have been carried out in more continental areas (e.g. Dietze et al., 2016; Lampe et al., 2009; Lorenz, 2007; Theuerkauf et al., 2022) and studies from the transition from maritime to continental conditions are rare (e.g. Lorenz, 2007). Moreover, many studies have been carried out on small lacustrine systems (e.g. Dreßler et al., 2011), in which anthropogenic impact often overprints natural climate variations (Haberzettl et al., 2019). These biases culminate in sometimes contradicting results, e.g. reconstructed lake-level curves, which have been used as key tools for hydroclimatic reconstructions (Kaiser et al., 2012). Apart from that, several studies from that area stress that not all observed lake-level variations are induced by climatic variations but rather by (anthropogenic) landcover changes influencing evapotranspiration and, consequently, groundwater recharge (e.g. Theuerkauf et al., 2022; Dietze et al., 2016).~~

~~In a wider regional context, hydroclimatic variability in the North Atlantic region during the Late Holocene has been related to changes in ocean circulations (e.g. Trouet et al., 2012; Bond et al., 2001), solar cycles (e.g. Martin-Puertas et al., 2012; Mellström et al., 2015) and atmospheric modes such as the NAO. The NAO is one of the leading atmospheric circulation systems influencing weather and climate conditions in the Northern Hemisphere (Bliedtner et al., 2023; Hurrell and Deser, 2009). It refers to changes in the atmospheric mass balance, i.e. the air pressure difference between the subpolar low (Iceland)~~

110 ~~and subtropic high (Azores) sea-level pressure (SLP) systems over the North Atlantic. These, in turn, influence surface air temperature, precipitation, and wind and storminess, including wind direction and storm tracks~~ (Hu et al., 2022). ~~NAO varies between two modes depending on the barometric difference between the pressure systems. A positive NAO (NAO+) is associated with a stronger gradient between the pressure systems causing zonal circulation and increased intensity of cyclones resulting, e.g. in stronger Westerlies~~ (Hurrell and Deser, 2009). ~~In contrast, a negative NAO (NAO-) has a weaker gradient~~

115 ~~causing a meridional circulation with weaker Westerlies, which results in more frequent atmospheric blocking and allows colder air from the Arctic regions to flow towards Europe~~ (Hurrell and Deser, 2009). ~~The NAO is more active in the cold season (October–April), with larger amplitudes and a strong influence on winter temperature and precipitation~~ (Hurrell et al., 2003). ~~Generally, a positive NAO is associated with mild and moist conditions (maritime), while a negative NAO is associated with cold and dry (continental) conditions in Central Europe~~ (Hurrell and Deser, 2009). ~~Recently, it has been suggested that~~

120 ~~winter conditions in the North Atlantic region can be linked to the combined effects of the NAO and the second mode of variability, i.e. the Eastern Atlantic pattern (EA) (e.g.~~ Comas-Bru and McDermott, 2014; Mellado-Cano et al., 2019). ~~The EA pattern is defined as sea-level pressure monopole between Iceland and Ireland (e.g.~~ Comas-Bru and McDermott, 2014; Moore et al., 2013) ~~modulating the location and intensities of the Icelandic Low and Azores High (e.g.~~ Moore et al., 2011) ~~consequently modulating e.g. the position of the North Atlantic storm tracks and jet stream~~ (Woollings et al., 2010; Seierstad

125 et al., 2007; Moore and Renfrew, 2012).

~~Coastal areas surrounding the Baltic Sea were identified as ideal for collecting proxy information about large-scale North Atlantic atmospheric patterns (e.g. the NAO) because temporal non-stationarities are neglectable there~~ (Comas-Bru et al., 2016). ~~To investigate the impacts of these large-scale atmospheric circulation patterns on North German lowlands, we identified Schweriner See (See = lake), a large hard-water lake located approximately 20 km south of the Baltic Sea and close~~

130 ~~to the boundary between more maritime to more continental climate, as a suitable archive that is not affected by the biases in previous studies in small lacustrine systems. As a rather large lake, Schweriner See is less susceptible to anthropogenic biases. Schweriner See has a relatively small catchment compared to its size~~ (Wöbbecke et al., 2003), ~~making it sensitive to hydrological changes.~~

2 Study Area

135 Schweriner See (53°43.256'N 11°27.544'E, 37.8 m a.s.l.) is ~~a hard-water lake~~ located in the North German lowlands in the westernmost part of the Mecklenburg Lake District ~~and approx. 20 km south of the Baltic Sea~~ (Fig. 1). The lake has a surface area of 61.54 km^2, extends over 24.8 km in ~~the~~ N-S direction and is up to 6 km wide in ~~the~~ E-W direction. Nowadays, Schweriner See has two similar-sized basins separated by an (in parts) artificial dam (Paulsdamm, Fig. 1B), which was built to connect the western and eastern shorelines in 1848 CE (Kasten and Rost, 2005). This was made possible by a lake-level

140 decline initiated by the broadening of the main outflow~~, of~~ the Stör waterway, which exposed the so-called Ramper Moor (Fig. 1). As a consequence, the previously periodically flooded Ramper Moor peninsula emerged as a calcareous mire

(Umweltministerium Mecklenburg-Vorpommern, 2003). The area of the dam is characterised by strong carbonate-rich groundwater inflow that results in an increased carbonate precipitation (Fig. 1D, Adolph et al., 2023; Umweltministerium Mecklenburg-Vorpommern, 2003). Before these construction activities, both lake basins were openly connected (Wiebeking, 1786), but today they are only linked by a small passage (Fig. 1). Both lake basins are characterised by complex morphometry with several deep areas, steep slopes, channel structures and extended shallow water areas (Fig. 1). The sediment core investigated in this study was taken in the deepest spot (52 m water depth, Fig. 1C) of the northern basin, the so-called Schweriner Außensee (SAS), which is characterised by a large shallow water area (< 5 m water depth) in the eastern littoral area susceptible to wave- and wind-induced dynamics (Fig. 1D, Adolph et al., 2023). This wide-spread shallow water area divides Schweriner Außensee into two subbasins in the south and north, whose depositional processes are mainly influenced by carbonate precipitation and productivity (Fig. 1, Adolph et al., 2023).

The overall catchment area is 414 km^2, but Schweriner Außensee comprises only 85 km^2. Overall, the catchment is mainly composed of farmland (47.5 %), water surfaces (20.9 %), forests (12.8 %), and populated areas (10.9 %) (Wöbbecke et al., 2003). The lake basin is mainly fed by groundwater (~70 %, pers. communication M. Lückstädt, Staatliches Amt für Landwirtschaft und Umwelt Westmecklenburg) and precipitation. Schweriner Außensee has only few small inflowing streams (Fig. 1C). Nowadays Schweriner See has two outflows passing ice marginal positions (IMP) of the Weichselian glaciation at the southern and northern end between which Schweriner See is located (Krienke and Obst, 2011). At the southern end, the river Stör drains through a valley formed by glacial meltwaters that broke through the southern IMP. The artificial Wallenstein trench was built in the 16th century at the northern end to connect Schwerin with the Baltic Sea. Naturally, Schweriner See discharges towards the North Sea by the river Stör. During the construction of the Wallenstein trench in the 16th century, the major natural watershed between the Baltic Sea and the North Sea was cut through, which most likely changed discharge characteristics and might have led to a decline in lake level (Adolph et al., 2022; Carmer, 2006). The lake water has a residence time of 11 years (Nixdorf et al., 2004).

The regional climate in northern Germany is characterised by a gradient with decreasing temperature and precipitation from west to east influenced by the strength and direction of the Westerlies, which are controlled by the respective mode of the NAO (Meinke et al., 2018). The climate at Schweriner See is affected by its location in the transition zone from a more maritime to a more continental climate. For the period 1991-2020, the climate near the study site, as shown by data from the closest weather station Schwerin, was characterised by a warm-temperate climate with a mean annual temperature of 9.5 °C, the coldest and warmest month being January (1.6 °C) and July (18.1 °C). Mean annual precipitation is 631 mm (DWD Climate Data Center, 2022b, 2022c) mean annual water balance is around 60 mm (1991-2000, DWD Climate Data Center, 2020). The main wind direction is W to SSW (1967-2022, DWD Climate Data Center, 2022a), resulting in a fetch of 6-8 km for Schweriner Außensee.

3 Material and Methods

3.1 Coring and Composite Profile

Two parallel sediment cores, SAS21-11 (13.56 m length) and SAS21-12 (15.51 m length) were obtained in September 2021 from the deepest part of Schweriner See (52 m water depth, Fig. 1) using a 90-mm inner diameter UWITEC piston corer (www.uwitec.at). Additionally, a short sediment surface core (SAS22-2, 77.5 cm length) was retrieved in July 2022 using a 60-mm inner diameter UWITEC gravity corer ~~(inner diameter: 60 mm)~~ to guarantee an intact surface. All sediment cores were transported to the Physical Geography laboratory of the University of Greifswald and stored under dark and cool (~4 °C) conditions before further processing. Sediment cores were split, and photographed, and sedimentological properties ~~and sediment colour~~ described according to standard protocols of the Physical Geography laboratory of the University of Greifswald. SAS22-2, SAS21-11 and SAS21-12 were spliced together using lithological marker layers, resulting in a composite sequence SAS21 of 17.76 ~~.5~~ cm length. ~~For this study, the upper 897.5 cm were investigated in detail.~~

3.2 Chronology

The chronology is based on 13 radiocarbon ages (Poznań Radiocarbon Laboratory) from terrestrial plant-macro fossils and 18 ^{210}Pb/^{137}Cs ages in the uppermost part of the composite profile. ^{210}Pb/^{137}Cs dating was carried out at the Environmental Radioactivity Research Centre of the University of Liverpool. Freeze-dried sediment samples from sediment core SAS22-2 were analysed for ^{210}Pb, ^{226}Ra, and ^{137}Cs by direct gamma assay in the Liverpool University Environmental Radioactivity Laboratory using Ortec HPGe GWL series well-type coaxial low background intrinsic germanium detectors (Appleby et al., 1986). ^{210}Pb was determined via its gamma emissions at 46.5 keV, and ^{226}Ra by the 295 keV and 352 keV γ-rays emitted by its daughter isotope ^{214}Pb following three weeks in storage in sealed containers to allow radioactive equilibration. ^{137}Cs was measured by its emissions at 662 keV. The absolute efficiencies of the detectors were determined using calibrated sources and sediment samples of known activity. Corrections were made for the effect of self-absorption of low energy γ-rays within the sample (Appleby et al., 1992). Unsupported (fallout) ^{210}Pb was calculated by subtracting ^{226}Ra concentrations from the total ^{210}Pb activities (Supplement S3-5). The age-depth model does not include the lowermost ^{210}Pb/^{137}Cs age, as only the upper 61 cm of sediment core SAS22-2 are part of the composite profile.

Except for this one age, all ages were used for age-depth modelling using the R-package 'rbacon' (v2.5.8, Blaauw and Christen, 2011) with the IntCal20 calibration dataset (Reimer et al., 2020) for calibration of radiocarbon data (Supplement S5-6). In the following, ages are reported as 'rbacon'-derived mean ages and the uncertainty is based on the ~~, including the~~ upper and lower limits of the 95 % confidence interval (Fig. 2). The sedimentation rate was calculated based on this age-depth model. For this study, only the upper 897.5 cm were investigated in detail as this depth marks the lowermost ^{14}C age and we refrained from extrapolating the age-depth model.

3.3 Scanning techniques

205 Spectral analysis on sediment cores was carried out directly on the cling wrap-covered freshly opened core surface using a Konica Minolta CM-2600d spectrophotometer (8 mm spot) in a 5 mm resolution (equivalent to a 0.5-3 year temporal resolution). The spectral composition was recorded with D65 at 10 nm steps from 360 nm to 760 nm wavelength. Sediment core colour was calculated from L*a*b* provided by the SpectraMagic NX software (Konica Minolta) to RGB using the R-package 'farver' (v2.1.1.9, Pedersen et al., 2022) and displayed on an age scale using Grapher (v20, Golden Software).

210 Hyperspectral imaging was carried out at the Université Rouen Normandie. Measurements were performed on U-channels previously extracted from the cores in Greifswald using a VNIR-PDF hyperspectral camera (SPECIM) and subsequently processed as described by Jacq et al. (2021) and van Exem et al. (2022). Images have a spatial resolution between 46x46 and 84x84 μm^2. Normalisation was carried out using the ENVI/IDL 5.5/8.2 software. Following van Exem et al. (2022), the spectral index $Area_{600-760}$ was used as an indicator for chloropigments indicating past *in-situ* productivity. To account for changes in

215 average reflectance induced by changes in carbonate content, $Area_{600-750}$ was normalised with the R_{mean}.

XRF-scanning was carried out at GEOPOLAR (Geomorphology and Polar Research) at the University of Bremen with an XRF Core Scanner (ITRAX, Cox Analytics) at 2-mm step size (equivalent to a 0.2-1.2 year temporal resolution) with a Mo tube (30 kV, 50 mA, 5 s exposure time). Scanning XRF-derived elemental variations might be influenced by sample geometry, physical properties (e.g. water content, surface roughness, grain size variations) or scanner settings (Croudace and Rothwell,

220 2010; Weltje and Tjallingii, 2008). To reduce such effects, only elements with less than 5 % zero values (Si, K, Ca, Ti, Mn, Fe, Ni, Cu, Zn, Sr) were centre log-ratio (clr) transformed (Aitchison, 1982) using the PAST 4 software (Hammer, 2022). As proposed by Adolph et al. (2023) Cu, Ni and Zn are used as a sum parameter $\sum(Cu,Ni,Zn)_{clr}$ for anthropogenic impact.

3.4 Sedimentological and ~~g~~Geochemical ~~a~~Analyses

Discrete samples were taken in a 1 cm resolution (equivalent to a 1-6 year temporal resolution) using LL-channels (Nakagawa,

225 2014). ~~Volume for dry-bulk density (DBD) was determined by the height and width of the LL- channels and sample resolution (V = 1 cm³ for SAS22-2 (upper 61 cm) and V = 3.24 cm³ for all other samples). DBD was calculated by dividing the dry weight of freeze-dried samples by the sample volume.~~ Loss-on-ignition (LOI) was determined on freeze-dried samples by heating the sediment to 550 °C for 3 h in a muffle furnace. Residues were used for grain size analysis. ~~and b~~ ~~Before processing for~~For grain size analysis, ~~, a few samples were investigated using microscopic analyses to determine the sample composition.~~

230 ~~C~~carbonates were removed with 5 ml HCl (10 %) and samples were dispersed overnight in an overhead shaker with 5 ml sodium pyrophosphate. Measurements were carried out using a Laser Particle Sizer (Fritsch Analysette 22 microtec plus). The first reproducible of nine subsequent runs was used for interpretation. Grain size statistics were calculated using the GRADISTAT 9.~~2~~1 software (Blott and Pye, 2001)~~(Blott and Pye, 2001)~~.

Carbonate content was determined on ground and homogenised samples by the Scheibler method on 0.17 to 0.55 g sample
235   material. Subtracting carbonate content and LOI_{550} from the total sample weight, the percentage of siliciclastics, which includes
a share of silicious algae as revealed by microscopic analyses on the LOI ash residues, was calculated.

Dried and homogenised sediment samples of 1.8 to 11.3 mg were used to analyse total carbon (TC) and total nitrogen (TN).
Concentrations were obtained using a Euro EA CNS analyser. TIC was determined with the IC Kit of the same device and
TOC was calculated as TOC = TC – TIC. Measurements were calibrated against certified reference materials. Error estimates
240   are based on triple measurements of 18 samples. The precision is 0.77-5.25 % for TN, 0.24-0.89 % for TC and 0.68-19.19 %
for TIC. The molar TOC/TN ratio was calculated based on molecular weights.

3.5 Leaf wax analyses

Leaf wax analyses were carried out at the Physical Geography department of the Friedrich-Schiller-University Jena. For this,
~~two~~one-centimetre-thick samples ~~for leaf wax analyses~~ were taken ~~to a 100-150 years resolution~~ and pooled with 0.5 cm of
245   sediment above and below the sampling depth resulting in a 100-150 year temporal resolution. Total lipids of the sediment
samples (2.5 to 9.1 g dry sediment) were extracted with 40 ml dichloromethane (DCM) and methanol (MeOH) (9/1, v/v) using
an ultrasonic bath over three 15-minute cycles. The total lipid extract was separated by solid phase extraction using
aminopropyl silica gel (Supelco, 45 μm) as the stationary phase. The n-alkanes were eluted with 4 ml hexane and further
purified using silver nitrate ($AgNO_3^-$; Supelco, 60-200 mesh). An Agilent 7890 gas chromatograph equipped with an Agilent
250   HP5MS column (30 m, 320 μm, 0.25 μm film thickness) and a flame ionisation detector (GC-FID) was used for identification
and quantification of the n-alkanes, relative to external n-alkane standards (n-alkane mix n-C_{21} - n-C_{40}, Supelco).

Compound-specific stable hydrogen isotope analyses were carried out for the n-alkanes C_{23} to C_{31} using an IsoPrime vision
IRMS coupled to an Agilent 7890A GC via a GC5 interface operating in pyrolysis modus with a MaxChrome and silver wool-
packed reactor at 1050 °C. The GC was equipped with a 30 m fused silica column (HP5-MS, 0.32 mm, 0.25 μm). Samples
255   were injected splitless with a split–splitless injector and each sample was analysed in triplicate. $\delta^2H_{n\text{-alkane}}$ was measured against
calibrated H_2 reference gas and all values are reported in per mille against VSMOW. The precision was checked by co-
analysing a standard alkane mixture (n-C_{27}, n-C_{29}, n-C_{33}) with known isotope composition (Arndt Schimmelmann, University
of Indiana), injected in duplicate every nine runs. All measurements were corrected for drift, relative to the standard values in
each sequence. n-C_{23} to n-C_{31} were abundant in sufficient amounts for compound-specific hydrogen analyses, but we will
260   focus on δ^2H_{C25} in the following. Triplicates for the δ^2H_{C25} had a standard deviation of <3.3‰, and the analytical error for the
standard duplicates was <1.1‰ (n = 9). The $H3^+$ factor was checked every two days and stayed stable at 3.59 ± 0.08 (n= 3)
during the measurements.

3.6 Pollen analyses

Altogether, 9189 samples with a one-centimetre thickness and ~~with a~~ 1-2 cm^3 volume were used for pollen analysis (equivalent
265   to a 16-85 year temporal resolution). Samples were treated with 10 % hydrochloric acid (HCl) to dissolve carbonates, heated

in 10 % potassium hydroxide (KOH) to remove humic compounds, and finally soaked in 40 % hydrofluoric acid (HF) for at least 24 h to remove the mineral fraction. Preparation was followed by acetolysis (Berglund and Ralska-Jasiewiczowa, 1986). One *Lycopodium* tablet (10679 spores; produced by Lund University) was added to the samples (Stockmarr, 1971). Sample slides were analysed using an ECLIPSE 50i upright 130 microscope and counted to at least 500 arboreal pollen (AP) grains. Pollen taxa were identified using atlases (Beug, 2004; Moore et al., 1991) and the reference grains owned by the Institute of Geoecology and Geoinformation, Adam Mickiewicz University, Poznań. Non-Pollen Palynomorph Image Database was used to identify NPPs (Shumilovskikh et al., 2022). Pollen percentages were calculated according to the formula: taxon percentage = (number of taxon grains/TPS) × 100%, where TPS indicates the total pollen sum including the AP and non-arboreal pollen (NAP) taxa, and excluding the local and spore-producing plants and NPP taxa.

3.7 Diatom analyses

For diatom analysis, 91 samples with a one-centimetre thickness and 1-2 cm^3 volume were taken in the same sampling resolution (equivalent to a 16-85 year temporal resolution) as the pollen analyses. At least 450 diatom valves were counted for each sample. Approx. 1 g of sediment was treated with HCl, H_2O_2, H_2SO_4 and $KMnO_4$ as described by Kalbe and Werner (1974). Residues were mounted on slides with Naphrax® to study them with a light microscope (Zeiss Axio Scope, oil-immersion Plan-Apochromatic objective, magnification 1000 X, numerical aperture 1.4). In total, 100 diatom samples were counted and at least 450 diatom valves were counted for each sample. Diatom species identification and classification as eutraphentic diatoms followed Krammer and Lange-Bertalot (1988, 1986, 1991a, 1991b), Krammer (1997a, 1997b, 2000, 2002, 2003), Lange-Bertalot (2001) and Lange-Bertalot et al. (2017; 2011). The abundance of eutraphentic diatoms was calculated as proposed by Adolph et al. (2023).

3.8 Statistics

Similar sedimentological and geochemical composition intervals were established using a stratigraphically constrained cluster analysis on clr-transformed XRF data and sedimentological parameters. XRF data were scaled to a 1-cm resolution calculating the mean for each centimetre to account for differences in resolution and noise between XRF scans and sedimentological data. Calculations were carried out using the R package 'rioja' (v. 1.0.5) (Juggins, 2022). As the cluster analysis did not cover some changes or would have led to many clusters, we included an additional unit boundary based on visual inspection (Unit C_1 to C_2). Pearson's r-values were calculated with the r-package 'Hmisc' (v. 5.0-1, Harrell Jr (2023)) (Supplement S1). Values with p < 0.001 are considered significant and are mentioned in the text.

4 Results

4.1 Lithology, chronology and sedimentation rate

295 Based on the hierarchical constrained cluster analysis result, the 897.5 cm long sediment sequence was subdivided into six major lithological units (A-F, Fig. 2). Unit C was subdivided into C_1 and C_2 based on changes in Ti_{clr} (Fig. 3) and D in three subunits (D_1-D_3) based on variations in the organic matter ~~variations~~ content (Fig. 2). Boundaries between units are mainly characterised by changes in organic matter content reflected, e.g.~~,~~ in sediment colour (Fig. 2) with lighter colours having an increased carbonate content and darker colour an increased organic matter content (e.g. Adolph et al., 2023; Strobel et al.,

300 2022a; Wündsch et al., 2016; Debret et al., 2011). Organic-rich sediment occurs from 878.5-844.5 cm sediment depth (Unit B) and, similarly, in Unit D_2 (Fig. 2). In contrast, carbonate content is ~~the~~ highest in Unit C. Otherwise, the sediment is composed of siliciclastic material, which includes ~~and~~ a share of diatoms and other silicious algae, ~~which~~ and is somewhat increased above 752.5 cm sediment depth marking the boundary between unit C_1 and C_2 (Fig. 2).

Bayesian age-depth modelling gave a ~~mean age~~ basal mean age of $3070^{+170}/_{-210}$ cal BP for the bottommost sample considered

305 for interpretation in this contribution (897.5 cm). All ages are in stratigraphic order and overlap with the 95 % confidence interval of the age-depth model (Fig. 2). The top~~most~~ age ~~of the composite profile~~ is determined by the recovery of the gravity core taken in ~~forming the top of the sequence (~~July 2022~~)~~. Total ^{210}Pb activity reached values close to equilibrium at 65 cm sediment depth. Concentration of the artificial radionuclide ^{137}Cs has a well-defined peak at 29-28 cm suggesting that this peak records fallout from the 1986 Chernobyl accident (Fig. 2). As t~~The~~ peak is well-resolved, it ~~Chernobyl ^{137}Cs peak~~ suggests

310 relatively little sediment mixing within this core. A smaller and less distinct peak at 45-44 cm may record the early 1960s fallout peak from the atmospheric testing of nuclear weapons. ~~The well-resolved Chernobyl ^{137}Cs peak suggests relatively little sediment mixing within this core.~~ The sedimentation rate is 2-3 mm a^{-1} between 897.5 cm ($3070^{+170}/_{-210}$ cal BP) and 298 cm ($620^{+35}/_{-50}$ cal BP) (Fig. 2) and increases to 4 mm a^{-1} at 56 cm ($7^{+10}/_{-10}$ cal BP). Above the record yields a much higher sedimentation rate of 5-10 mm a^{-1}.

315 **4.2. Sediment composition**

~~Indicators for minerogenic input (~~Ti_{clr} and K_{clr}~~, r =0 .79,~~ Davies et al., 2015; Haberzettl et al., 2005~~)~~ show a significant positive correlation (r =0 .79, Fig. 3). Ti_{clr} is partly in agreement with grain size mean (r = 0.54), which is mostly related to variations in sand content (r = 0.94), though, not all Ti_{clr} maxima are reflected in the grain size mean. ~~The g~~Grain size mean~~s~~ range~~s~~ from 11.56-56.98 µm with maximum values at the transition from ~~u~~Units A~~-B~~ to B~~-~~, in ~~U~~units D_2 and F. Maximum grain size mean

320 is characterized by an increased share of the sand fraction >125 µm of up to 21.5 % (Fig. 3). Parameters for organic matter content, LOI_{550}, TOC, TN and inc/coh, are significantly correlated (r > 0.70, Supplement S1) ranging from 8.1-65.5 %, 4.6-20.3 % and 0.07-2.2 % ~~respectively~~. All agree visually well with *in-situ* chloropigments (Area$_{600-760}$~~,~~ (Fig. 3). Additionally, Sr/Ca is significantly correlated with, e.g. inc/coh, (r = 0.80) or LOI_{550} (r = 0.62). Values are highest in units B and D_2 and minimal in units C and E. TOC/N is mostly <12 ~~ranges~~ ranging ~~from~~ between 6.2-21.6 ~~with maximum~~ except for higher values

325 in units C_1 and F. mMinimum values in are observed in unit E. The individual and summed (C_{21}-C_{35}) *n*-alkane concentrations correlate with the organic matter parameters of Schweriner See (r > 0.8, Supplement S2). *n*-alkane concentration ranges from 6.9-42.1 ng g^{-1} with maximum values in units B and D2 and minimum values in units C_2 and E. δ^2H_{C25} shows a similar pattern as δ^2H_{C23-31} and ranges from -171.9 ± 1.17 ‰ to -1511.9696 ± 0.05 ‰ being minimal in units C and F and having a maximaum in units B, D_2 and E. Ca, Sr and TIC as indicators for carbonate precipitation (Haberzettl et al., 2005; Haberzettl et al., 2019;

330 Haberzettl et al., 2009) are significantly correlated to each other but are negatively correlated to LOI_{550}, TOC, TN and inc/coh productivity indicators (r > -0.76). Consequently, values are lowest in units B and D_2 and highest in units C and E with TIC and carbonate values ranging from 0.1-7.2 % and 8.4-69.8 %, respectively.

Diatom abundance is characterized by planktonic diatoms from between 50.6-90.1 % with maximum values in units B and F and minimum values between units B and C. Eutraphentic diatoms are range from ~11.7 % (1.4 to 22.5 %) in uUnits A-E.

335 AfterwardsAbove, they increase significantly up to 92.1 % in Unit F. $\sum(Cu,Ni,Zn)_{clr}$ is correlated to eutraphentic diatoms (r = 0.63). The diatoms species *S. chantaicus* Genkal & Kuzmina occurss only in uUnits C and E concurrently with minima in the inc/coh ratio (Fig. 4). Pollen composition is characterized by a dominance of arboreal pollen (AP) from between 77.37-98.91 % with maximum valuesa in Uunits C_1 and D_2 and minimaum values in uUnits E and F. $\sum$(*Carpinus betulus, Fagus sylvatica*) ranges between from 1.3-39 % with a maximum in uUnit D2 and minimum values in Uunits A-C_2 and F.

340 $\sum(Cu,Ni,Zn)_{clr}$ is correlated to eutraphentic diatoms (r = 0.63), and both reflect human impact.

5 Interpretation

5.1 Productivity Organic matter and δ^2H as indicators for NAO-related hydroclimatic variability

5.1.1 Organic matter as an indicator for winter temperature variability

Traditionally parameters for organic matter content in lake sediments (e.g. LOI_{550}, TOC, TN and inc/coh) in lake sediments

345 are are either interpreted indicative of changes in the organic matter preservation and/or as indicators for organic matter preservation and/or in-lake productivity (e.g. Dräger et al., 2017; Hodell and Schelske, 1998). In our record, parameters for organic matter content (As at Schweriner See , LOI_{550}, TOC, TN and inc/coh), are significantly correlated to each other (r > 0.70, Supplement S1) to each other, but significantly negatively correlated to parameters indicating carbonate precipitation Ca, Sr and TIC (Ca, Sr and TIC, r > -0.76,), which indicate carbonate precipitation Haberzettl et al., 2005;

350 Haberzettl et al., 2019; Haberzettl et al., 2009) Since $Area_{600-760}$ reflects *in-situ* chloropigments (e.g. van Exem et al., 2022), we consider LOI_{550}, TOC, TN and inc/coh as indicative for in-lake productivity, which is supported by TOC/TN values mostly < 12 indicative for a dominance of nonvascular aquatic plants with only a small contribution of vascular plants (Meyers and Ishiwatari, 1993). Moreover, the individual and summed (C_{21}-C_{35}) *n*-alkane concentrations correlate with the in-lake productivity of Schweriner See (r > 0.8, Supplement S2), indicating a predominance of in-situ aquatically derived *n*-alkanes

355 (e.g. Strobel et al., 2022b; Sachse et al., 2004). The compound-specific isotopic hydrogen signatures (δ^2H) of the *n*-alkanes

C_{22} to C_{31} show a comparable pattern (Supplement S2), further indicating a predominantly aquatic origin of the *n*-alkanes (e.g. Strobel et al., 2022b; Sachse et al., 2004), thiswhich suggestings that one suite of parameters dilutes the other. Organic matter parameters agree visually well with *in-situ* chloropigments (Area$_{600-760}$, Fig. 3), which are indicative of past primary productivity (van Exem et al., 2022), and TOC/N ratio mostly <12, which suggests a dominance of nonvascular aquatic plants

360 with only a small contribution of vascular plants (Meyers and Ishiwatari, 1993). Therefore, we consider the organic matter content as an indicator for in-lake productivity. As organic matter parameters agree visually well with Area$_{600-760}$ (Fig. 3), which are indicative for in-lake productivity (van Exem et al., 2022), this .Therefore, we consider our the organic matter content as indicator for variability in in-lake produktivity. This is supported by the significant correlations between the Sr/Ca ratio and organic matter content parameters. T(e.g. inc/coh, r = 0.80). he Changes in Sr/Ca ratio suggests changes in the

365 carbonate precipitation mechanism towards between biogenically calcite precipitation (= higher Sr/Ca) and inorganic calcite precipitation (= lower Sr/Ca), because biogenically precipitated calcite has higher Sr contents than inorganically precipitated calcite (Hodell et al., 2008). Phases ofAs, the higher Sr/Ca ratios (Iincreased biogenic calcite precipitationbiological carbonate precipitation) (Sr/Ca ratio) occurs duringcoincide with phases of higher organic matter content, whichthis supporting supports our conclusion that organic matter content is driven by in-lake productivity rather than being a preservation signal (Fig. 3).

370 Moreover, itthis suggests that inorganic carbonate precipitation might be the background sedimentation in Schweriner See diluted by changes in productivity. However, biogenicallybiologically-induced calcite precipitation during high-productivity periods may have additionally enhanced the organic matter preservation (Hodell and Schelske, 1998). In the following, inc/coh will be used as in-lake productivity signal because this parameter has the highest resolution.

375 SubsequentlOfteny, changes in iproductivity are often related to changes in temperature and/or nutrient availability (Kasper et al., 2013; Günther et al., 2016; Doberschütz et al., 2014). In our recordAt Schweriner See, Tthe abundance of eutraphentic diatoms, whichis indicative for of increased nutrient availability andy, correlates to $\sum(Cu,Ni,Zn)_{clr}$ (r = 0.63), which both indicates suggest an according to previous studies increaseding anthropogenic impactforcing, namely eutrophication and contamination respectively correlated to eutrophication and contamination respectively (Adolph et al., 2023). But Since since

380 the abundance of eutraphentic diatoms (Fig. 4) indicates suggests an increase increased nutrient availability only after 105^{+95}_{-75} cal BP (unit F, Fig. 4), we consider major anthropogenic forcings on the lake productivity asunlikely before. WWe rather suggested und conclude that productivity was driven by temperature variability (units A-E) beforehand. The influence of Ttemperature variations on in-lake productivity is supported by the recurrent occurrence of the diatom species *S. chantaicus*, which occurs concurrently withduring low productivity phases (r = 0.54, Fig. 4). *S. chantaicus* grows underneath the ice-cover

385 and is associated with long-lasting ice cover duration until the spring months (Scheffler and Padisák, 2000). Such Llong-lasting ice-covers under colder winter conditions may substantially affect the seasonal heat budget, timing and length of stratification but also the productivity of aquatic ecosystems (e.g. Bonsal et al., 2006) because long-lasting ice covers delay the onset of the growing season and/or reduce water temperatures, which results in a reduced productivity of the lake system. ContraryIn contrast, during milder winter temperatures the growing season may start earlier and surface water temperatures may already

hat formatiert: Schriftart: Kursiv

390 be increased, which prolongs the growing season and results in a higher productivity of the lake system. ~~Such an effect of long-lasting ice-cover duration on the in-lake productivity is the concurrent occurrence of *S. chantaicu*s occurs lyr = 0.54,~~ Based on the sample thickness for diatom analysis of one centimetre, which covers 1-6 years depending on the sedimentation rate, it is not possible to distinguish between individual years. However, the regularity in the occurrence of *S. chantaicus* suggests that the occurrence is not triggered by single events but rather by long-lasting changes in environmental conditions,

395 which is also supported by long-lasting phases of lower productivity during which *S. chantaicus* occurs (units C and E, Fig. 4).

Therefore, we ~~conclude~~suggest that before $105^{+95}/_{-75}$ cal BP in-lake productivity was mainly driven by winter temperature variability modulating ice cover duration, and consequently, heat budget and growing season length (e.g. Schmidt et al., 2019; Bonsal et al., 2006; Blenckner et al., 2007). In the following, inc/coh as organic matter parameter will be used as winter

400 temperature signal because this parameter has the highest temporal resolution (Fig. 4).

5.1.2 δ^2H as indicators for moisture source changes and/or evaporative enrichment

Regarding *n*-alkanes, lacustrine sediments generally contain a mixed signal from terrestrial and aquatic sources, which can be distinguished by their chain-length distribution (e.g. Strobel et al., 2021; Ficken et al., 2000). Classically, long-chain *n*-alkanes (e.g. C_{27}-C_{31}) are suggested to be produced as leaf waxes by higher terrestrial plants and primarily incorporate the local growing

405 season precipitation as their primary source water for photosynthesis (e.g. Sachse et al., 2012; Strobel et al., 2020; Strobel et al., 2022a). However, the δ^2H signal of precipitation mainly depends on the atmospheric moisture source of the precipitation in the mid-latitudes (Strobel et al., 2020; Strobel et al., 2022b; Bliedtner et al., 2020; Wirth and Sessions, 2016). Also additional fractionation processes can occur at the plant-soil interface, with the evaporation of soil water and transpiration of leaf water being prominent factors (Feakins and Sessions, 2010; Kahmen et al., 2013; Zech et al., 2015). In contrast, short-chain *n*-alkanes

410 are produced by aquatic macrophytes and algae (e.g., C_{21}-C_{25}) and incorporate the δ^2H signal of the lake's water, which integrates the δ^2H precipitation signal throughout the year. Depending on the morphometric and hydrological parameters of the lake itself, lake water can be strongly modulated by evaporative lake water enrichment (e.g. Aichner et al., 2022; Mügler et al., 2008; Sachse et al., 2004; Strobel et al., 2022a). Notably, this classic *n*-alkane source attribution (terrestrial vs aquatic) is not always trivial because, for example, aquatic emergent plants can also synthesize distinct amounts of long-chain *n*-alkanes

415 ($\geq C_{27}$), which then also incorporate the δ^2H signal of the lake's water, challenging the interpretation of the δ^2H signal (Ficken et al., 2000; Yang and Bowen, 2022).

~~In our record, t~~The correlations between individual and summed (C_{21}-C_{35}) *n*-alkane concentrations ~~correlate~~ with the organic matter parameters of Schweriner See ~~(r > 0.8, Supplement S2),~~ ~~indicating~~indicate a predominance of *in-situ* aquatically-derived *n*-alkanes (e.g. Strobel et al., 2022b; Sachse et al., 2004). This is supported by the molar TOC/TN values ~~are~~mostly

420 < 12 indicating a dominance of nonvascular aquatic plants with only a small contribution of vascular plants (Meyers and Ishiwatari, 1993). The comparable pattern of compound-specific isotopic hydrogen signatures (δ^2H) of the *n*-alkanes C_{23} to C_{31} ~~show a comparable pattern~~ (Supplement S2), further ~~indicating~~indicate a predominantly aquatic origin of the *n*-alkanes

(e.g. Strobel et al., 2022b; Sachse et al., 2004) and we therefore suggest that the majority of the *n*-alkanes is of aquatic origin. Although the compound-specific δ^2H of all detectable *n*-alkanes shows a comparable pattern, mixing can complicate the interpretation of the longer-chained *n*-alkanes and we will therefore focus on δ^2H of C_{25} (δ^2H_{C25}) in the following because C_{25} and its δ^2H signal provide the most robust aquatic end-member. δ^2H_{C25} is more enriched during periods of higher productivity (= milder winter temperatures) and more depleted during periods of lower productivity (= colder winter temperatures, Fig. 4), which can be due to the following two explanations: i) Since the aquatically-derived δ^2H_{C25} primarily reflects δ^2H of the lake's water and year-round precipitation, Schweriner See's position in the mid-latitudes suggests that δ^2H_{C25} is mostly related to moisture source changes in the North Atlantic region. More enriched δ^2H_{C25} values may correspond to isotopically enriched southern/central North Atlantic moisture sources (Fig. 1A). In contrast, more depleted δ^2H_{C25} values originate from isotopically depleted moisture sources from the northern North Atlantic and/or Arctic region. On the other hand, ii) enriched δ^2H_{C25} could also result from temperature-driven evaporative lake water enrichment, as frequently reported from semi-arid regions (Mügler et al., 2008; Strobel et al., 2022a) with a higher evaporative lake water enrichment during warmer temperatures and a lower evaporative lake water enrichment during colder temperatures. ~~instudy sites ,the mean annual water balance indicates is a negative water balace while compared to Schweriner See shows a positive water balance, . Additionally, lake water evaporation in these lakes shows spatially vaying amplitudes and seems to depend on the lakes morphological parameters and hydrological features (Aichner et al., 2022). Similar to Schweriner sSee, deep lakes with high water residence times and absence of river connections show low lake water enrichment while shallow lakes with low water volume experience high lake water enrichment (Aichner et al., 2022).~~

~~All this explains that thus lake water has an increased in shallower lakes in southeast Germany compared to thereSchweriner See~~

5.1.3 NAO variability

~~region~~Based on the in-lake ~~the~~ productivity, the occurrence or disappearance of the diatom species *S. chantaicus*, both reflecting changes in winter temperature, as well as variations in the compound-specific hydrogen isotopes, reflecting changes in the moisture source region (Fig. 1A) and/or evaporative lake water enrichment, we observe four distinct time slices: ~~P~~hases with i) warmer winter temperatures, a southern moisture source region in the southern North Atlantic and/or a higher evaporative lake water enrichment from $3030^{+170}/_{-210}$-$2820^{+180}/_{-180}$ cal BP (unit A-B, Fig. 4) and $2110^{+160}/_{-130}$-$830^{+100}/_{-90}$ cal BP (unit D, Fig. 4), and contrary, ii) colder winter temperatures, a northern moisture source in the northern North Atlantic and/or Arctic regions and/or lower evaporative lake water enrichment from $2820^{+180}/_{-180}$-$2110^{+160}/_{-130}$ cal BP (unit C, Fig. 4) and $830^{+100}/_{-90}$-$105^{+95}/_{-75}$ cal BP (unit E, Fig. 4). ~~, and ii) iP~~ Such distinct variations in winter temperatures, moisture source region and/or evaporative lake water enrichment are mainly modulated by the North Atlantic Oscillation (NAO) in the North Atlantic region (Hurrell and Deser, 2009) because the barometric difference between high- and low-pressure systems over the Azores and Iceland affects Westerly strength and pathways and eventually the moisture source region (Fig. 1A). Milder winter temperatures are associated with a NAO+ initiated by strong high- and low-pressure systems over the Azores and Iceland

resulting in strong Westerlies, which bring moist and mild air from the southern North Atlantic with precipitation enriched in δ^2H (e.g. Breitenbach et al., 2019; Hurrell, 1995; McDermott et al., 2011; Baldini et al., 2008; Comas-Bru et al., 2016). In contrast, during NAO- conditions, pressure systems are weakened, which allows a frequent atmospheric blocking redirecting the Westerlies southward and a frequent intrusion of cold and dry air from northern North Atlantic and Arctic regions with

460   precipitation depleted in δ^2H (e.g. Breitenbach et al., 2019; Hurrell, 1995; McDermott et al., 2011; Baldini et al., 2008; Comas-Bru et al., 2016). Still, temperature changes may at least partly drive the evaporative lake water enrichment.
~~.~~ Considering this interpretation, time slices from 3030^{+170}/$_{-210}$-2820^{+180}/$_{-180}$ cal BP and 2110^{+160}/$_{-130}$-830^{+100}/$_{-90}$ cal BP are interpreted as NAO+ conditions. Conversely, time slices from 2820^{+180}/$_{-180}$-2110^{+160}/$_{-130}$ cal BP and 830^{+100}/$_{-90}$-105^{+95}/$_{-75}$ cal BP correspond to NAO- phases (Fig. 5). Rates of changes between positive ~~to~~and negative conditions vary between the

465   individual phases, e.g. with a rapid drop in winter temperature around 2820^{+180}/$_{-180}$ cal BP but a~~n~~ gradual increase from 2110^{+160}/$_{-130}$-1720^{+70}/$_{-70}$ cal BP (Fig. 5).

5.2~~5.2~~ Minerogenic input as an indicator for various interacting processes

~~Indicators for minerogenic input (Ti$_{elr}$ and K$_{elr}$, r =0 .79, Davies et al., 2015; Haberzettl et al., 2005) show a significant positive~~
~~correlation. Often, Ti is associated with silty sediments (e.g. Davies et al., 2015; Kylander et al., 2011), but here, Ti$_{elr}$ is partly~~

470   ~~in agreement with grain size mean (r = 0.54), which is mostly related to variations in sand content (r = 0.94). In the following,~~
~~Ti$_{elr}$, which has a lower signal-to-noise ratio than K, will be used as minerogenic input indicator.~~

~~In particular, t~~The correlated **5.2.1 Processes affecting minerogenic input**

m~~inerogenic~~ elements titanium and potassium are often regarded as a proxy for minerogenic input from the catchment (Haberzettl et al., 2005; Haberzettl et al., 2019; Davies et al., 2015). ~~, which both show a significant positive correlation to~~

475   ~~each other (Ti$_{elr}$ and K$_{elr}$, r =0 .79). Often, Ti is associated with silty sediments (e.g. Davies et al., 2015; Kylander et al., 2011),~~
~~but here, Ti$_{elr}$ is partly in agreement with grain size mean (r = 0.54), which is mostly related to variations in sand content (r =~~
~~0.94).~~ Therefore, M~~m~~inerogenic input is either ~~associated with two main interpretations, i.e.~~ windier and/or wetter conditions (Davies et al., 2015). Normally, one would expect that under increased windiness, the minerogenic input increases because an additional aeolian component would be introduced to the lake. However, this is unlikely for our record because Schweriner

480   Außensee is surrounded by a cliff on the western shoreline (Fig. 1) serving as a wind shelter, and pollen composition suggests a closed canopy forest (AP pollen, Fig. 4) inhibiting aeolian erosion and transport. Moreover, under wetter conditions, one would expect an increased minerogenic input because an increased surface run-off would bring more allochthonous material into the lake (Haberzettl et al., 2007). However, Schweriner See has hardly any above-ground inflow and is mainly fed by groundwater (Wöbbecke et al., 2003), which has no impact on particulate minerogenic matter transport. Therefore, wetter

485   conditions result in higher lake levels but without an increased minerogenic matter supply to the coring location.
As aeolian input and above-ground inflow are of minor importance for Schweriner Außensee (Wöbbecke et al., 2003), we suggest that minerogenic input is mainly modulated by the unique morphometry of the lake basin, which is characterized by a

broad, shallow water area in front of the eastern shoreline (Fig. 1C). We assume this area ~~as a~~to be the main source for minerogenic material as surface sediment sampling revealed highest values for minerogenic elements there (e.g. Ti, K, Adolph et al., 2023). During higher (lower) lake levels, the shallow water area would be further away (closer) from the coring site, which results in a reduced (higher) transport of wave-eroded minerogenic material towards the coring site. Our interpretation of minerogenic matter ~~input~~supply as a shoreline distance indicator is supported by previous investigations on (paleo)lacustrine landforms (e.g. beach ridges, nearshore bar) on the north-eastern shoreline of Schweriner See (Adolph et al., 2022), which indicate higher lake-level phases during ~~phases of~~ reduced ~~lower~~ minerogenic input at our coring site ~~for~~at 3020 ± 260, 330 ± 50 and 260 ± 40 BP (OSL)~~. These high lake levels coincide with lower minerogenic input at our coring site~~. In contrast, lower lake level phases are implied for 1050-950 BP (archaeological findings, Konze, 2017; Lorenz et al., 2017), 585 ± 75 BP (OSL, Adolph et al., 2022), and 120-100 BP (historical documents, Umweltministerium Mecklenburg-Vorpommern, 2003) coinciding with a higher minerogenic ~~input~~matter supply to SAS21 (Fig. 5). Support for the interpretation of Ti_{clr} as shoreline distance indicator ~~comes~~derives from the ~~minerogenic elements K and Ti, which~~ partly ~~correlat~~eion of the minerogenic elements K and Ti to the grain size mean. Both grain size mean ~~or~~and median ha~~s~~ve previously been used in large lakes as a paleo-shoreline distance indicator, e.g. Kasper et al. (2012) arguing that during episodes of higher lake levels – and therefore a larger paleo-shoreline distance of the coring location – coarser grains did not reach the coring location. Similar suggestions have been made by Bonk et al. (2023) for Lake Lubińskie, where ~~under~~during lower water levels, shorelines were exposed and more susceptible to erosion and, consequently, Ti and quartz grains increased at the coring location.

However, ~~However,~~ due to a fetch of 6-8 km, ~~this area~~the eastern shoreline of Schweriner See is highly susceptible to wind-induced wave action, which might have affected the sensitivity of Ti_{clr} as lake level ~~proxy sensitivity~~indicator. Therefore, ~~m~~Due to the proposed input mechanism, the ~~M~~minerogenic ~~input~~matter supply may ~~therefore~~ additionally be influenced by i) wind speed changes and increased storminess, which controls wave energy and, consequently, the amount of material eroded and transported, and ii) wind directional changes modulating ~~the~~ fetch and shoreline distance. We assume that ~~S~~such changes ~~are~~should be reflected in the grain size mean, which only partly correlates to Ti_{clr}, with a reworking of coarser grains during periods of intensified wind disturbance. Therefore, sections with high Ti_{clr} ~~values~~content in combination with coarser grain sizes do not ~~always~~necessarily correspond to lower lake levels but could also be triggered by increased wind-induced wave action ~~influence~~. Compared to other phases with a similarly high Ti_{clr} content, ~~The~~ the grain size mean is~~, in particular,~~ly increased at the transition from units A to B ~~and unit D_{2}~~. ~~During these phases, the grain size mean and sand content are significantly increased compared to other phases with a similar Ti_{clr} content, which indicates the input of coarser grains~~particles and, ~~consequently~~likely, higher wave energy likely related to stronger winds. One of these instances when wind speed enhanced the Ti_{clr} signal is at $3020^{+180}/_{-210}$-$2940^{+190}/_{-200}$ cal BP and in unit D_{2} from $1660^{+40}/_{-50}$-$1120^{+90}/_{-100}$ cal BP (Fig. 5). Concurrently with the first interval, a nearshore bar (3020 ± 260 BP (OSL)) was deposited at the north-eastern shoreline, which first of all indicates a higher lake level as it was deposited up to 1.2 m above today's lake level (Adolph et al., 2022). However, within the sediment sequence of this nearshore bar, several layers of very coarse grains (> 2 mm) were deposited, which is only possible under high wave energy driven by increased wind speed. ~~I~~This is in accordance~~,~~ with a ~~larger~~higher percentage

of sand ~~was introduced to the coring location~~ at the distal coring location of SAS21. ~~These~~is ~~phases with increased sand are consistent with NAO+ conditions, which are associated with stronger winds and increased storminess.~~ Similarly, the period from $1660^{+40}/_{-50}$ ~~cal BP~~ $1120^{+90}/_{-100}$ cal BP has a high Ti content suggesting a lower lake-level but also an increased Sand$_{>125\mu m}$

signal, which likely masked the shoreline distance signal. Therefore, the concurrently increased minerogenic input is most likely related to strongly increased wind-induced wave energy. Consequently, to reliably infer the shoreline distance, ~~Therefore, the~~ Ti$_{elr}$ signal has to be evaluated against the grain size mean and Sand$_{>125\mu m}$ ~~content~~ as an indicator ~~of~~ for wind speed changes, which might sometimes dominate the ~~Ti$_{elr}$~~ signal ~~instead of the shoreline distance~~. Finally, both phases of increased sand are consistent with NAO+ conditions (Fig. 5), which are associated with stronger winds and increased storminess supporting the interpretation of the coarser grain sizes.

~~Largely,~~

~~Tt~~These interpretations have been made under the assumption of today's prevailing wind direction from SW to W, which results in a fetch of 6-8 km. However, changing wind directions to more northerly and easterly wind directions might have also influenced ~~the~~ erosional processes. Under such conditions the minerogenic input to the coring location would be increased because the coring location is closer to the western than the eastern shoreline (Fig. 1). Under prevailing northerly or easterly winds, wave action would have increased at the western shoreline, which might have increased minerogenic input and would falsely suggest a lower lake level. However, northerly to easterly winds are associated with drier conditions in NE Germany and~~,~~ ~~T~~therefore, minerogenic ~~input~~matter supply might reflect a lower lake level due to drier conditions and a decreased shoreline distance due to changes in the prevailing wind direction. In conclusion, the main drivers for minerogenic input to the coring location of SAS21 at Schweriner See are shoreline distance variations with additional wind speed influences amplifying wave action, particularly under NAO+ conditions. ~~In the following, Ti$_{elr}$, which has a lower signal-to-noise ratio than K, will be used as an indicator for shoreline distance.~~

~~5~~6 Discussion

~~5.1 Hydroclimatic variations influenced by NAO polarity~~5.1.1 Productivity and δ^2H as Indicators for NAO-related hydroclimatic variability

~~In-lake productivity, exemplified by the inc/coh ratio in Fig. 4 as it has the highest resolution, is often interpreted as either controlled by temperature and/or nutrient input~~ (Kasper et al., 2013; Günther et al., 2016; Doberschütz et al., 2014). ~~As the abundance of eutraphentic diatoms suggests an increase in eutrophication only after $105^{+95}/_{-75}$ cal BP ($1845^{+75}/_{-95}$ CE) (Unit F, Fig. 4), productivity was likely driven by temperature variability before. Distinct temperature changes are supported by the recurrent occurrence of the diatom species S. chantaicus, which is associated with long-lasting ice covers~~ (Scheffler and Padisák, 2000) ~~concurrent with low productivity phases (Fig. 4). Such prolonged ice covers indicate lower winter temperatures and longer lake ice-cover duration, which can substantially affect the seasonal heat budget, timing and length of stratification but also the productivity of aquatic ecosystems (e.g.~~ Bonsal et al., 2006). ~~Therefore, we conclude that before $105^{+95}/_{-75}$ cal BP in-lake productivity was mainly driven by winter temperature variability modulating ice cover duration, heat budget and growing season length, most likely modulated by large-scale atmospheric patterns (e.g.~~ Schmidt et al., 2019; Bonsal et al., 2006; Blenckner et al., 2007). ~~Similar observations of winter~~

temperatures influencing in-lake productivity by modulating ice-cover duration and growing season length have been made for a lake in western-central Sweden (Czymzik et al., 2023).

Regarding *n*-alkanes, lacustrine sediments generally contain a mixed signal from terrestrial and aquatic sources, which can be distinguished by their chain-length distribution (e.g., Strobel et al., 2021; Ficken et al., 2000). Classically, long-chain *n*-alkanes (e.g., C₂₇-C₃₁) are suggested to be produced as leaf waxes by higher terrestrial plants and primarily incorporate the local growing season precipitation as their primary source water for photosynthesis (e.g., Sachse et al., 2012; Strobel et al., 2020; Strobel et al., 2022a). However, the δ²H signal of precipitation mainly depends on the atmospheric moisture source of the precipitation in the mid-latitudes (Strobel et al., 2020; Strobel et al., 2022b; Bliedtner et al., 2020; Wirth and Sessions, 2016) and also additional fractionation processes can occur at the plant-soil interface, with evaporation of soil water and transpiration of leaf water being prominent factors (Feakins and Sessions, 2010; Kahmen et al., 2013; Zech et al., 2015). In contrast, short-chain *n*-alkanes are produced by aquatic macrophytes and algae (e.g., C₂₁-C₂₅) and incorporate the δ²H signal of the lake's water, which integrates the δ²H precipitation signal throughout the year. Depending on the morphometric and hydrological parameters of the lake itself, lake water can be strongly modulated by evaporative lake water enrichment (e.g., Aichner et al., 2022; Mügler et al., 2008; Sachse et al., 2004; Strobel et al., 2022a). Notably, this classic *n*-alkane source attribution (terrestrial vs aquatic) is not always trivial because, for example, aquatic emergent plants can also synthesize distinct amounts of long-chain *n*-alkanes (≥C₂₇), which then also incorporate the δ²H signal of the lake's water, challenging the interpretation of the δ²H signal (Ficken et al., 2000; Yang and Bowen, 2022)

At Schweriner See, *n*-alkane concentration, as well as individual *n*-alkanes and their respective δ²H signals, are significantly correlated with in-lake productivity indices (Fig. 3; Supplement S1-S2) and we therefore suggest that the majority of the *n*-alkanes is of aquatic origin. Although the compound-specific δ²H of all detectable *n*-alkanes shows a comparable pattern, mixing can complicate the interpretation of the longer-chained *n*-alkanes and we will therefore focus on δ²H of C₂₅ (δ²H_{C25}) in the following because C₂₅ and its δ²H signal provide the most robust aquatic end-member. δ²H_{C25} is more enriched during periods of higher (milder) winter temperatures and more depleted during periods of colder winter temperatures (Fig. 4), which can be due to the following two explanations: i.) Since the aquatically-derived δ²H_{C25} primarily reflects δ²H of the lake's water and year-round precipitation, Schweriner See's position in the mid-latitudes suggests that δ²H_{C25} is mostly related to moisture source changes in the North Atlantic region. More enriched δ²H_{C25} values may correspond to isotopically enriched southern/central North Atlantic precipitation sources. In contrast, more depleted δ²H_{C25} values originate from isotopically depleted precipitation from the northern North Atlantic and/or Arctic region. On the other hand, ii.) enriched δ²H_{C25} could also result from temperature-driven evaporative enrichment of the lake water, as frequently reported from semi-arid regions (Mügler et al., 2008; Strobel et al., 2022a). Such observations have also been made for several smaller lakes from northeastern Germany (Aichner et al., 2022). However, these lakes are located ca. 120 km southeast of Schweriner See in the more continental climate zone where evaporative enrichment may have an increased influence on the isotopic composition of lake water.

Such distinct variations in winter surface air temperatures, precipitation sources, and/or evaporative enrichment are mainly modulated by the North Atlantic Oscillation (NAO) in the North Atlantic area (Hurrell and Deser, 2009). The barometric difference between high- and low-pressure systems over the Azores and Iceland affects Westerly strength and pathways and eventually the moisture source for northern Central Europe. Milder winter temperatures are associated with NAO+ initiated by strong high- and low-pressure systems over the Azores and Iceland resulting in strong Westerlies, which bring moist and mild air from the southern North Atlantic with more positive δ²H values to northern Central Europe (e.g., Breitenbach et al., 2019; Hurrell, 1995; McDermott et al., 2011; Baldini et al., 2008; Comas-Bru et al., 2016). In contrast, during NAO- conditions, pressure systems are weakened, which allows frequent atmospheric blocking redirecting the Westerlies southward and a frequent intrusion of cold and dry air from northern North Atlantic and Arctic regions, which is associated with more negative δ²H values (e.g., Breitenbach et al., 2019; Hurrell, 1995; McDermott et al., 2011; Baldini et al., 2008; Comas-Bru et al., 2016). Still, changes in winter temperature may at least partly drive evaporative enrichments with higher enrichment during milder winter temperature phases,

reflecting a positive NAO and, conversely, lower enrichment coinciding with colder winter temperatures linked to a negative NAO.

Considering this interpretation, from $3030^{+170}/_{-210}$-$2820^{+180}/_{-180}$ cal BP and $2110^{+160}/_{-130}$-$830^{+100}/_{-90}$ cal BP, milder winter temperatures (inc/coh, Fig. 5) and more enriched δ^2H_{C25} are interpreted as NAO+ conditions. Northward displaced westerlies bring isotopically enriched precipitation from the southern/central North Atlantic to northern Central Europe and/or warmer temperatures may result in a higher evaporative environment. Conversely, from $2820^{+180}/_{-180}$-$2110^{+160}/_{-130}$ cal BP and $830^{+100}/_{-90}$-$105^{+95}/_{-75}$ cal BP, colder winter temperatures with prolonged ice cover duration and more depleted δ^2H_{C25} values correspond to negative NAO phases. Westerlies are displaced southward and a more frequent atmospheric blocking allows for the intrusion of northerly winds with precipitation from the northern Atlantic and Arctic region and/or colder temperatures (Fig. 5). Rates of changes between positive to negative conditions vary between the individual phases e.g. with a rapid drop in winter temperature (inc/coh) around $2820^{+180}/_{-180}$ cal BP but an gradual increase from $2110^{+160}/_{-130}$-$1720^{+70}/_{-70}$ cal BP (Fig. 5).

~~5~~6.1.~~2~~ NAO variability during the past ~~3 ka~~3000 years on an interregional scale

A comparison to other NAO-sensitive records from Greenland (Olsen et al., 2012), Norway (Faust et al., 2016), Scotland (Baker et al., 2015), Sweden (St. Amour et al., 2010) and Germany (Waltgenbach et al., 2021), ~~(e.g.~~Faust et al., 2016; Baker et al., 2015; St. Amour et al., 2010; Breitenbach et al., 2019; Waltgenbach et al., 2021; Olsen et al., 2012~~)~~which reflect~~ing past NAO variations~~ NAO variability, shows a~~ are in good agreement with signals from our record (Fig. 5). ~~Moreover, data from the precipitation sensitive record from Dosenmoor (ca. 105 km northwest of Schweriner See, Fig. 5,~~ Barber et al., 2004; Charman et al., 2009~~, Fig. 5) aligns well with changes in the moisture source region. As expected under a positive NAO influence, a southern moisture source region causes wetter conditions. In comparison, a northern moisture source region under negative NAO conditions causes drier conditions (Fig. 5) due to shifts in the westerly pathway.~~

Similar to our record, ~~positive~~ NAO+ conditions were inferred ~~for~~ from $3030^{+170}/_{-210}$-$2820^{+180}/_{-180}$ cal BP ~~were inferred~~ for Central Scandinavia (St. Amour et al., 2010) and Greenland (Olsen et al., 2012) (Fig. 5). Subsequent ~~negative~~NAO- conditions ~~corresponds from $2820^{+180}/_{-180}$-$2110^{+160}/_{-130}$ cal BP are also in accordance with~~to predominantly ~~negative NAO~~negative NAO conditions reconstructed from various other records from $2820^{+180}/_{-180}$-$2110^{+160}/_{-130}$ cal BP (Olsen et al., 2012; Becker et al., 2020; Faust et al., 2016; Baker et al., 2015; St. Amour et al., 2010) (Fig. 5). ~~In addition to this t~~These negative NAO conditions~~, for the North Atlantic region, a~~coincide with an overall shift to cooler conditions and/or wetter and/or windier conditions (e.g. Engels et al., 2016; Martin-Puertas et al., 2012; Rach et al., 2017; van Geel et al., 2014; van Geel et al., 2000; Mellström et al., 2015; Harding et al., 2023; Martínez Cortizas et al., 2021), which ~~occur~~occurred in the North Atlantic region ~~occurred~~ around 2800 cal BP (2.8 ka event) and was ~~-~~attributed to changes in solar activity (Homeric ~~Grand Solar m~~Minimum, ~2800–2550 cal BP, Reimer et al., 2020). ~~Generally~~In addition to the cooler conditions, this period is ~~also~~ linked to cooler and/or wetter and/or windier conditions (e.g. Engels et al., 2016; Martin-Puertas et al., 2012; Rach et al., 2017; van Geel et al., 2014; van Geel et al., 2000; Mellström et al., 2015; Harding et al., 2023; Martínez Cortizas et al., 2021).~~ The onset of the Homeric ~~Grand Solar m~~Minimum (2800 cal BP) is within the error range of observed cooler conditions ($2820^{+180}/_{-180}$ cal BP) at Schweriner See. ~~Generally, this period is linked to cooler and/or wetter and/or windier conditions (e.g.~~Engels et al., 2016; Martin-Puertas et al., 2012; Rach et al., 2017; van Geel et al., 2014; van Geel et al., 2000; Mellström et al., 2015; Harding et al., 2023; Martínez

Cortizas et al., 2021). These changes in solar activity These changes in solar activity triggered a a rapid climate change and
640 likely changes in atmospheric circulation patterns. , which are linked to cooler and/or wetter and/or windier conditions (e.g.
Engels et al., 2016; Martin-Puertas et al., 2012; Rach et al., 2017; van Geel et al., 2014; van Geel et al., 2000; Mellström et al.,
2015; Harding et al., 2023; Martínez Cortizas et al., 2021). Some studies associate solar minima with shifts to a negative NAO
conditions (e.g. Shindell et al., 2001; Gray et al., 2016), as observed in this study at Schweriner See. Other studies suggest a
weakening of the subpolar gyre, resulting in changes in the atmospheric circulation, for example, by more frequent and
645 persistent atmospheric blocking (Moffa-Sánchez et al., 2014), as it would also be observed under negative NAO conditions.
Sjolte et al. (2018) suggest a complex response to solar minima, which is not directly linked to the NAO but rather to the
Eastern Atlantic pattern with increased mid-Atlantic blocking and shifts to intensifying northerly winds resembling negative
NAO conditions. Such Sshifts in the Eastern Atlantic pattern during gGrand Ssolar Mminima are supported by Harding et al.
(2023) for the North Sea region.
650 At
For Schweriner See, colder winter temperatures, a more northern moisture source region from the northern North Atlantic
and/or Arctic regions and/or low temperatures driving evaporative lake water enrichment low evaporative lake water
enrichment is inferred until 2110^{+155}/$_{-130}$ cal BP, indicating prevailing negative NAO conditions beyond the Homeric Grand
Solar MinimaMinimum. A similar phenomenon with cooler conditions for 2800-1650 cal BP was also observed at close-by
655 Rugensee (Dreßler et al., 2011). Contemporaneously, for 2550-2050 BP (OSL), dominating northerly to easterly winds are
reported between 2550-2050 BP (OSL) (Lampe and Lampe, 2018) for the close-by Darss area (ca. 110 km northeast of
Schweriner See, Lampe and Lampe, 2018), which are also commonly associated with negative NAO conditions. observed in
SAS21 and A similar phenomenon with cooler conditions were observed for 2800-1650 cal BP was also observed at close-by
Rugensee for 2800-1650 cal BP (Dreßler et al., 2011). .
660 The A shift to warmer positive NAO conditions from 2110^{+160}/$_{-130}$-830^{+100}/$_{-90}$ cal BP with a gradual increase in winter
temperature until 1720^{+70}/$_{-70}$ cal BP coincides with the Roman Warm Period (RWP, c. 2150-1550 cal BP), which was a period
of general warmth and dryness in Europe (Lamb, 2013). Similarly, shifts to positive NAO+ conditions have beenwere
reconstructed from different archives from Scotland (Baker et al., 2015), Norway (Faust et al., 2016) and Central Scandinavia
(St. Amour et al., 2010) (Fig. 5), St. Amour et al., 2010; Baker et al., 2015; Faust et al., 2016) and considering chronological
665 uncertainties, it is in accordance agreement with NAO reconstructions from Greenland (Olsen et al., 2012) suggesting a
predominantly stable positive NAO circulation pattern from 2000-550 cal BP. Contemporaneously, a change in forest
composition occurs (Fig. 4Fig. 4), most likely induced by milder and moister winter conditions leading to optimal climatic
conditions for the expansion of beech (*Fagus sylvatica*) and hornbeam (*Carpinus betulus*) also observed at Schweriner See as
both maxima coincide with higher winter temperatures (Fig. 3, Fig. 4, e.g. Bradshaw et al., 2010). However, anthropogenic
670 activities, e.g., soil changes, cannot be excluded from these species' spread (Giesecke et al., 2017).
Predominantly negative NAO conditions between 830^{+100}/$_{-90}$-105^{+95}/$_{-75}$ cal BP are contemporaneous with a long-term cooling
trend associated with repeated phases of volcanic-solar downturns in Europe (PAGES 2k Consortium, 2013). Compared to the

previous negative NAO phase, which coincides with lower solar activity, this period shows a stable low winter temperature but repeated shifts to a northern moisture source region and/or low temperature driven lake water evaporative lake water enrichment, e.g. around $860^{+95}/_{-95}$ and $540^{+65}/_{-90}$ cal BP. Considering chronological uncertainties, both shifts might also align again to Grand Ssolar Mminimas, i.e. the Oort (940-880 cal BP) and Spörer (560-400 cal BP) solar minima (Usoskin et al., 2007). From 800-500 BP (OSL), the negative NAO conditions are confirmed supported by frequent strong winds from northern and eastern directions (Lampe and Lampe, 2018). After $105^{+95}/_{-75}$ cal BP the temperature signal is masked by eutrophication dominating in-lake productivity (Adolph et al., 2023), which is why it is not possible to link the reconstruction to monitoring data (e.g. ice cover duration).

5.2 Minerogenic input as an indicator for various interacting processes

5.2.1 Processes affecting minerogenic input

Minerogenic elements titanium and potassium are often regarded as a proxy for minerogenic input from the catchment (Haberzettl et al., 2005; Haberzettl et al., 2019) associated with two main interpretations, i.e. windier and/or wetter conditions (Davies et al., 2015). Normally, one would expect that under increased windiness, the minerogenic input increases because an additional aeolian component would be introduced to the lake. However, this is unlikely for our record because Schweriner Außensee is surrounded by a cliff on the western shoreline (Fig. 1) serving as a wind shelter, and pollen composition suggests a closed canopy forest (Fig. 4) inhibiting aeolian erosion and transport. Moreover, under wetter conditions, one would expect an increased minerogenic input because an increased surface run-off would bring more allochthonous material into the lake (Haberzettl et al., 2007). However, Schweriner See has hardly any above-ground inflow and is mainly fed by groundwater, which has no impact on particulate minerogenic matter transport. Therefore, wetter conditions result in higher lake levels but without a minerogenic matter supply to the coring location. Higher lake levels are, for example, indicated by paleo-lacustrine landforms (e.g. beach ridges, nearshore bar) from the north-eastern shoreline of Schweriner See (Adolph et al., 2022) for 3020 ± 260, 330 ± 50 and 260 ± 40 BP (OSL). However, such high lake levels coincide with lower minerogenic input in SAS21. In contrast, phases of lower lake levels are implied for 1050-950 BP (archaeological findings, Konze, 2017; Lorenz et al., 2017), 585 ± 75 BP (OSL, Adolph et al., 2022), and 120-100 BP (historical documents, Umweltministerium Mecklenburg-Vorpommern, 2003) coinciding with a higher minerogenic input to SAS21 (Fig. 5).

As aeolian input and above ground inflow are of minor importance for Schweriner Außensee (Wöbbecke et al., 2003), we suggest that minerogenic input is mainly modulated by the unique morphometry of the lake basin, which is characterized by a broad, shallow water area in front of the eastern shoreline (Fig. 1B). We assume this area as a main source for minerogenic material as surface sediment sampling revealed highest values for minerogenic elements there (e.g. Ti, K, Adolph et al., 2023). This area is highly susceptible to wind-induced wave action as it is exposed to the main wind direction with a fetch of 6-8 km. During higher (lower) lake levels, the shallow water area would be further away (closer) from the coring site, which results in a reduced (higher) transport of wave-eroded minerogenic material towards the coring site. Further support for this interpretation comes from the good correlation of minerogenic elements K and Ti to grain size mean. Both grain sizes mean or medians have previously been used in large lakes as a paleo-shoreline distance indicator, e.g. Kasper et al. (2012) arguing that during episodes of higher lake levels — and therefore a larger paleo-shoreline distance of the coring location — coarser grains did not reach the coring location. Similar suggestions have been made by Bonk et al. (2023) for Lake Lubińskie, where under lower water levels, shorelines were exposed and more susceptible to erosion and, consequently, Ti and quartz grains increased at the coring location.

In the following, Ti$_{clr}$, which has a lower signal-to-noise ratio than K, will be used as minerogenic input indicator mainly depending on paleo-shoreline distance related to lake level changes (Fig. 5).

As a second factor, minerogenic input is also controlled by wind-induced wave action, wind speed and direction changes, which might have affected proxy sensitivity. Wind speed and storminess changes probably influenced minerogenic input as this controls wave energy and, consequently, the amount of material eroded and transported. Therefore, wind activity might sometimes dominate the Ti signal instead of the lake level. One of these instances when wind speed and storminess on Schweriner See dominated Ti deposition at SAS21 could be at 3020 ± 260 BP (OSL) when a nearshore bar investigated by Adolph et al. (2022), indicates both a high lake-level phase with windy conditions. Several layers of very coarse grains (> 2 mm) were deposited within this nearshore bar, which is only possible under high wave energy driven by increased wind speed. In accordance, increased storminess was suggested for the Danish North Sea coast between 3300-2800 BP (Goslin et al., 2018) and SW Sweden from 3050-2850 BP (Björck and Clemmensen, 2004). Therefore, the concurrently increased minerogenic input (3020^{+180}/$_{-210}$-2940^{+190}/$_{-200}$ cal BP, Fig. 5) is likely related to strongly increased wind-induced wave energy. In contrast to storminess affecting the minerogenic input, an actual lower lake level for this period is supported by drier conditions at Dosenmoor during the nearshore bar deposition (Fig. 5), supporting our initial paleo-shoreline proximity interpretation. However, the sediment sequence of the nearshore bar suggests continuous sedimentation with no evidence of post-depositional erosion (Adolph et al., 2022). This inconsistency could be resolved if a drop in lake level concurrent with stormier conditions is assumed. Such a drop may lead to the deposition and preservation of the nearshore bar and a higher Ti input due to both processes, i.e. windier conditions and a subsequent lower lake level.

The interpretation of minerogenic input as a relative lake-level indicator is based on today's prevailing wind direction from SW to W, which results in a fetch of 6-8 km. However, changing wind directions to more northerly and easterly wind directions might have also influenced the erosional processes. Consequently, minerogenic input to the coring location of SAS21 at Schweriner See would be reduced because the coring location is closer to the western than eastern shoreline (Fig. 1). Such a change in wind direction was, for example, reconstructed for the close-by Darss area (Lampe and Lampe, 2018). Under prevailing northerly or easterly winds, wave action would have increased at the western shoreline, which might have increased minerogenic input, suggesting a lower lake level even if only the wind direction changed. However, northerly to easterly winds are associated with drier conditions in NE Germany. Therefore, minerogenic input might reflect a lower lake level due to drier conditions and a decreased shoreline distance due to changes in the prevailing wind direction.

To test the reliability of Ti$_{clr}$ as a proxy for shoreline distance (i.e. lake-level variations), it is compared bog surface wetness reconstructions from peat bog Dosenmoor (ca. 105 km northwest of Schweriner See, Fig. 5, Barber et al., 2004; Daley and Barber, 2012) both mirroring moisture availability in the following. Bog surface wetness is assumed to reflect the summer moisture deficits mainly driven by precipitation but reinforced by temperature (Charman et al., 2009). Similar processes affecting the lake level at Schweriner See have been observed recently. For example, a summer moisture deficit due to prevailing dry conditions in 2018 resulted in a severe lake-level decline (Landesamt für Umwelt, Naturschutz und Geologie Mecklenburg-Vorpommern, 2018), which could not be completely compensated by winter precipitation. Therefore, we suggest that bog surface wetness is a suitable proxy for comparison. For the past 3000 years, higher and lower lake level phases derived from Schweriner See align well with reconstructed wetter and drier conditions at Dosenmoor (Fig. 5, Barber et al., 2004) in all but one instances, i.e. the period from 1660^{+40}/$_{-50}$-1120^{+90}/$_{-100}$ cal BP. For this period, a lower lake level is suggested by Ti$_{clr}$ (Fig. 5), indicating drier conditions, which contrasts with hydroclimatic reconstructions from Dosenmoor (Daley and Barber, 2012), other records (Magny, 2004; Büntgen et al., 2021; Starkel et al., 2013, Fig. 6) and our NAO reconstruction implying a positive NAO associated with milder and wetter conditions at the same time (Fig. 5). However, positive NAO conditions are also associated with an enhanced storm activity (e.g. Hurrell et al., 2003), which is in accordance with stormier conditions during the period of interest in Northwest Europe from 1700-1100 cal BP (Pouzet et al., 2018) and 1900-1050 cal BP (Sorrel et al., 2012) and in

southwestern Sweden around 1500 cal BP (Jong et al., 2007; Jong et al., 2006). Therefore, we assume increased storminess masked our lake level signal for this period.

In conclusion, the main driver for minerogenic input to the coring location of SAS21 at Schweriner See were lake-level variations with additional wind speed influences and direction amplifying wave action. Consequently, the lake level was higher than today for 3070^{+170}/$_{-210}$-2380^{+170}/$_{-150}$ cal BP. Afterwards, the lake level was lower for 2380^{+170}/$_{-150}$-2050^{+130}/$_{-110}$ cal BP before it rose again until 1660^{+40}/$_{-50}$ cal BP. For 1660^{+40}/$_{-50}$ cal BP-1120^{+90}/$_{-100}$ cal BP, the lake-level signal was most likely masked by increased storminess and might have been higher than today. A lower lake level for 1050^{+90}/$_{-70}$-850^{+100}/$_{-90}$ cal BP, which aligns with a suggested lake level of at least 2 m below today's for the same period (Konze, 2017; Lorenz et al., 2017). This phase is followed by a higher lake level from 850^{+100}/$_{-90}$-650^{+40}/$_{-40}$ cal BP and a lower lake level from 650^{+40}/$_{-40}$-410^{+95}/$_{-110}$ cal BP, which coincides with peat deposits below today's lake level around 530^{+35}/$_{-25}$ cal BP (Adolph et al., 2022). A higher lake level is indicated for 410^{+95}/$_{-110}$-210^{+105}/$_{-95}$ cal BP supported by two beach ridge deposits dated 330 ± 50 and 260 ± 40 BP (OSL). The subsequent lake-level decline concurs with the construction of the so-called Wallensteingraben in the 16th century, which was built to connect Schweriner See with the Baltic Sea. By establishing a second outflow, the outflow regime was likely changed (Carmer, 2006; Adolph et al., 2022). The expansion of the Stör waterway in the mid-19th century also resulted in a lower lake level (Fellner, 2007; Umweltministerium Mecklenburg-Vorpommern, 2003), which resulted in the division into two lake basins we see today (Fig. 1).

6.2.2 Lake-level variability reflected in the sediments **of Schweriner See**

6.2.1 Lake-level variability at Schweriner See Evaluating the reliability of minerogenic input as a lake-level indicator

To reliably assign lake-level variations, also consider

Our interpretation of minerogenic input as a lake-level indicator is supported by previous investigation (paleo)lacustrine landforms on the north-eastern shoreline of Schweriner See (Adolph et al., 2022), which indicate previous phases of higher lake levels for around Theseat our coring site, which partly correlate the

wind speed and changes in wind direction changes have to be considered at Schweriner See changes into account. One of these instances of wWindier conditions contemporaneously with a higher lake level indicated by a nearshore bar (Adolph et al., 2022) were inferred for Schweriner See for 3020^{+180}/$_{-210}$-2940^{+190}/$_{-200}$ cal BP. supported by the nearshore bar deposition were inferredenhanced theei signal is at (. Concurrently, a nearshore bar () was deposited at the north-easternshoreline, which first of all indicated a higher lake level (Adolph et al., 2022). Wthe sediment sequence of this , sSuch increased storminess is in accordance with records from the Danish North Sea coast between 3300-2800 BP (Goslin et al., 2018) and SW Sweden from 3050-2850 BP (Björck and Clemmensen, 2004) and our reconstruction of NAO+ conditions. However, the reconstructed higher lake level at Schweriner See is in contrast to a hydroclimatic reconstruction from Dosenmoor (ca. 105 km northwest of Schweriner See, Fig. 5, Barber et al., 2004; Daley and Barber, 2012), which suggests drier conditions during this period (Fig. 5). Observations at Dosenmoor are in line with and is suggested by the reconstructed positive NAO, which is associated with increased storm activity. most However (ca. 105 km northwest of Schweriner See, Barber et al., 2004; Daley and Barber, 2012)our initial paleo-shoreline proximity interpretation of Ti$_{elr}$ (Fig 5). This inconsistency could be resolved if a drop in lake level concurrent with stormier conditions is assumed. Such a drop may lead to the deposition and preservation of the nearshore bar and a higher Ti supply due to both processes, i.e. windier conditions and a subsequent lower lake level (Fig. 5). This is supported by the sediment succession in the nearshore bar itself, which suggests a rapid continuous sedimentation with no

evidence of post-depositional erosion (Adolph et al., 2022). Another period of windier conditions is suggested also from $1660^{+40}/_{-50}$ cal BP-$1120^{+90}/_{-100}$ cal BP (Fig. 5), which agrees with similar observations from Northwest Europe from 1700-1100 cal BP (Pouzet et al., 2018) and 1900-1050 cal BP (Sorrel et al., 2012) as well as from southwestern Sweden around 1500 cal BP (Jong et al., 2007; Jong et al., 2006) and our NAO+ reconstruction.

To further test the reliability of Ti_{clr} as a proxy for shoreline distance (i.e. lake-level variations), it iswe continue to compared that parameter to bog surface wetness reconstructions from peat bog Dosenmoor (ca. 105 km northwest of Schweriner See, Fig. 5, Barber et al., 2004; Daley and Barber, 2012) both mirroring moisture availability in the following.: Bog surface wetness is assumed to reflect the summer moisture deficits mainly driven by precipitation but reinforced by temperature (Charman et al., 2009). Similar processes affect the lake level at Schweriner See and have been observed recently. For example, a summer moisture deficit due to prevailing dry conditions in 2018 resulted in a severe lake-level decline (Landesamt für Umwelt, Naturschutz und Geologie Mecklenburg-Vorpommern, 2018), which could not be completely compensated by winter precipitation. Therefore, we suggest that bog surface wetness is a suitable proxy for comparison. For the past 3000 years, higher and lower lake level phases derived from Schweriner See align well with reconstructed wetter and drier conditions at Dosenmoor (Fig. 5, Barber et al., 2004) in all but one instances, i.e. the period from $1660^{+40}/_{-50}$-$1120^{+90}/_{-100}$ cal BP, where our Ti_{clr} shoreline distance signal was masked by increased storminess. Considering that wetter conditions were widely reconstructed for several European records (Magny, 2004; Büntgen et al., 2021; Starkel et al., 2013, Fig. 6) and that our record suggests NAO+ conditions, it is likely that the lake-level was higher at Schweriner See as well.

In conclusionTherefore, we infer the following lake level history for Schweriner See: ,the lake level was higher than today for $3070^{+170}/_{-210}$-$2380^{+170}/_{-150}$ cal BP. AfterwardsSubsequently, the lake level was lower for $2380^{+170}/_{-150}$-$2050^{+130}/_{-110}$ cal BP before it rose again until $1660^{+40}/_{-50}$ cal BP. For $1660^{+40}/_{-50}$ cal BP-$1120^{+90}/_{-100}$ cal BP, the lake-level signal was most likely masked by increased storminess and might have been higher than today. A lower lake level ofat $1050^{+90}/_{-70}$-$850^{+100}/_{-90}$ cal BP also aligns with a suggested lake level of at least two meters below today'sthe modern one for the same periodbased on archaeological findings at Schweriner See (Konze, 2017; Lorenz et al., 2017). This phase is followed by a higher lake level from $850^{+100}/_{-90}$-$650^{+40}/_{-40}$ cal BP and a lower lake level from $650^{+40}/_{-40}$-$410^{+95}/_{-110}$ cal BP, which coincides with peat deposits below today's lake level around $530^{+35}/_{-25}$ cal BP (Fig. 5, Adolph et al., 2022). A higher lake level is indicated for $410^{+95}/_{-110}$-$210^{+105}/_{-95}$ cal BP and supported by two beach ridge deposits dated to 330 ± 50 and 260 ± 40 BP (OSL, Adolph et al., 2022). The subsequent lake-level decline concurs with the construction of the Wallensteingraben in the 16th century (Fig. 1), which was built to connect Schweriner See with the Baltic Sea. By establishing a second outflow, the outflow regime was therefore likely changed (Carmer, 2006; Adolph et al., 2022). Previously the second outflow, the Stör waterway, likely had no significant influence on the lake-level because, for example, around 1830 CE, the river was so shallow that sit was difficult to navigate the Stör even with boats with shallow drafts (Ruchhöft, 2017). Only the expansion of the Stör waterway in the mid-19th century resulted in a lower lake level there (Fellner, 2007; Umweltministerium Mecklenburg-Vorpommern, 2003), which resulted in the division into the two lake basins we see today (Fig. 1).

hat formatiert: Tiefgestellt

wetter conditions reconstructed from, whichimplies +an increase in the grain size mean suggests increased (wind-induced) wave actions, which aligns with +. This is

830 sare, particularly under NAO+ conditions,wind al changesof6.2.23 Late Holocene regionalDriving mechanisms for lake-level variations

Discrepancies between the NAO record and the shoreline distance may occur due to the different forcings. The NAO is most active during the cold season month (October – April) and mostly influences winter hydroclimate in Central Europe. Contrary, lake-level variability is additionally influenced by summer moisture deficits, e.g. due to drier summer conditions, which may

835 result in lake-level declines that cannot be compensated even by rainy winter conditions, which has been observed recently (Adolph, 2024). Such trends are supported by the general alignment of Llower lake levels generally align with a northern moisture source region (Fig. 5Fig. 5) associated with drier winters, which indicates that winter precipitation may have a noticeable influence on lake-level variations. Similarly, This is in accordance with modelling approaches by Vassiljev (1998), who suggested that lakess in temperate humid areas are likely highly more sensitive to changes in winter precipitation

840 compared to summer precipitation and winter precipitation and that lake-level changes from lakes, which are large in comparison to their catchment like Schweriner See, are more likely to reflect changes in precipitation.

In general, lake-level variations observed at Schweriner See agree with patterns observed in different archives (e.g. lacustrine sediments, peat bogs, tree rings) reflecting lake-level variations and hydroclimatic conditions in Denmark (Barber et al., 2004), NE-Germany (Daley and Barber, 2012; Theuerkauf et al., 2022), western Poland (Pleskot et al., 2018; Bonk et al., 2023;

845 Starkel et al., 2013) but also Eastern Central Europe (Büntgen et al., 2021) and the Jura mountains (Magny, 2004) (Fig. 6). Offsets might occur due to chronological uncertainties, proxy sensitivity and/or additional local to regional influences. For example, some studies Theuerkauf et al. (2022) and Bonk et al. (2023) argue for more local to regional influences on Late Holocene lake level during the Late Holocenes by identifying (anthropogenic) landcover changes and forest structures as partly responsible for lake-level variations (e.g. Theuerkauf et al., 2022; Bonk et al., 2023; Dietze et al., 2016). In particular, a

850 (anthropogenically induced) change between forested and open vegetation landscapes was linked to an altered changed groundwater recharge and, consequently, higher lake levels under more open vegetation for Tiefer See (~75 ha, ca. 70 km east of Schweriner See, Theuerkauf et al., 2022). Such local-to-regional influences could have led to varying onsets of lake-level high stands, particularly for smaller lake systems, which are more susceptible to local and regional (anthropogenic) influences. For example, for at small Lake Lubińskie (22.7 ha, ca. 275 km southeast of Schweriner See), it is stressed that lake-level

855 variations are mainly related to anthropogenic activity within the catchment (Bonk et al., 2023), which may explain the difference to large Schweriner See. Additional influences, which might lead to different onsets, might be the hydro(geo)logical network or different climatic settings concerning such as for example increasing continentality from west to east (Bonk et al., 2023). For Schweriner See, we suggest that i) (anthropogenically) induced landcover changes had a minor influence because the pollen composition of Schweriner See suggests a closed canopy forest cover until 665^{+40}_{-30} cal BP and ii) additional such

860 local effects were dampened by the lake's size.

As hydroclimatic conditions at Schweriner See have been influenced by NAO variability, most likely, regional lake-level variations have at least partly been driven by large-scale changes in atmospheric circulation systems as well. For example, lower lake levels tend to coincide with a negative NAO, which is associated with drier winter conditions (Fig. 5). Similarly, modelling approaches by Vassiljev (1998) suggest that lakes in temperate humid areas are more sensitive to changes in winter precipitation (e.g. NAO variability) compared to summer precipitation. The influence of large-scale atmospheric changes on lake-level variability during the past 3000 years explains the similar lake-level variations and hydroclimatic conditions in different archives (Fig. 6). Discrepancies between the NAO-related parameters, i.e. winter temperature and moisture source region, and the shoreline distance, i.e. lake level, at Schweriner See (Fig. 5) may occur due to sometimes independent forcing mechanisms. NAO is most active during the cold season month (October – April) and mostly influences winter hydroclimate in Central Europe whereas lake-level variability is additionally influenced by summer moisture deficits, e.g. due to drier summer conditions. This may result in lake-level declines that cannot be compensated even by rainy winter conditions, which was observed e.g. after dry summer conditions in 2018 and 2022 (Adolph, 2024). Normally, such summer moisture deficits should be reflected in δ^2H_{C25} if the isotopic lake water composition is driven by evaporative lake water enrichment and would then show a similar pattern as shoreline distance and bog surface wetness from Dosenmoor (Fig. 5, Daley and Barber, 2012), as both are related to changes in precipitation and evapotranspiration. Such influences of evaporative lake water enrichment have been observed for several smaller lakes in north-eastern Germany (Aichner et al., 2022). However, these study sites are located ca. 120 km southeast of Schweriner See in the more continental climate zone, whereas Schweriner See is located in the transition zone between maritime and continental climate. These areas differ by their mean annual water balance, which is negative in northeast Germany but slightly positive at Schweriner See (Adolph, 2024) suggesting an increased evaporative lake water enrichment in lakes east of Schweriner See. Moreover, lake water evaporation in these lakes shows spatially varying amplitudes and seems to depend on the lake's morphological parameters and hydrological features (Aichner et al., 2022). Additionally, lakes similar to Schweriner See, i.e. deep lakes with high water residence times and absence of river connections, show low evaporative lake water enrichment (Aichner et al., 2022). Because δ^2H_{C25} mostly correlates to winter temperature changes at Schweriner See (Fig. 5), we suggest that the δ^2H_{C25} predominantly depends on moisture source changes in the North Atlantic region potentially explaining differences in the NAO and lake-level reconstructions. Still, an additional influence of evaporative lake water enrichment cannot be completely excluded.

Additional (supra-)regional drivers may have affected lake-level variability as well. For example, changes in the solar activity are suggested to be one key driver for Holocene hydroclimatic variability in the Jura mountains, where higher lake levels were linked to lower solar activity (Magny, 2004). However, this explanation can only partly be applied to Schweriner See (Fig. 5) and other compared records (Fig. 6). We rather observe temporal offsets between low solar activity and higher lake levels when comparing records from, e.g. Lake Lubińskie (Bonk et al., 2023), Lake Strzeszyńskie (Pleskot et al., 2018) and Tiefer See (Theuerkauf et al., 2022), which might be a result of complex spatial ocean-land interactions as a response to solar activity as suggested by Swindles et al. (2007). For Schweriner See only a few periods of a higher lake level

895 align with solar minima, e.g. the Homeric ~~Grand Solar~~ Minim~~um~~a (2800–2550 cal BP, Fig. 5, Fig. 6). After the 12th century, anthropogenic interferences, e.g. weirs, the building of mills or the construction of the Wallenstein trench may have influenced the lake level beyond natural variations.

7 Conclusions

Sediments obtained from Schweriner See are a valuable archive for studying Late Holocene environmental variability. Due to
900 its size, local (anthropogenic) effects are dampened and proxies reflect large-scale climatic variations, which align well with interregional paleoclimatic reconstructions covering the ~~Late Holocene~~past 3000 years. Before $105^{+95}/_{-75}$ cal BP (~1850 CE), in-lake productivity in Schweriner See was mainly ~~influenced~~ driven by winter temperature variability, which modulates ice cover duration and growing season length~~.~~ ~~R~~resulting in lower productivity during colder periods and~~, vice versa,~~ higher productivity during warmer periods. Changes in ~~The c~~Cwinter temperature and ~~the~~ moisture source region (δ^2H_{C25}) covary: i)
905 milder winter temperatures ~~align~~coincide with a southern moisture source region, and, ii) colder winter temperatures ~~and~~with a northern moisture source region. These distinct variations enable the reconstruction of large-scale atmospheric processes, suggesting NAO polarity as a driver.~~Afterwards, anthropogenic impact on Schweriner See increased significantly, resulting in in-lake productivity mainly driven by nutrient supply (eutrophication).~~
~~Winter temperatures and changes in the moisture source region covary enable the reconstruction of large-scale atmospheric~~
910 ~~processes, suggesting NAO polarity as a driver.~~ Positive NAO conditions are characterized by ~~increased productivity~~milder winter temperatures and a southern moisture source region due to stronger Westerlies bringing warm, moist air towards northwest Europe, which occurred from $3030^{+175}/_{-215}$-$2820^{+180}/_{-180}$ cal BP and $2110^{+155}/_{-130}$-$830^{+100}/_{-90}$ cal BP. In contrast, conditions resembling a negative NAO ~~(cold and dry) are~~ associated with ~~lower productivity~~colder winter temperatures and a northern moisture source region occur ~~can be reconstructed for~~at $2820^{+180}/_{-180}$-$2110^{+155}/_{-130}$ cal BP and $830^{+100}/_{-90}$-$105^{+95}/_{-75}$ cal
915 BP. ~~Positive NAO conditions occurred from $3030^{+175}/_{-215}$-$2820^{+180}/_{-180}$ cal BP and $2110^{+155}/_{-130}$-$830^{+100}/_{-90}$ cal BP, while negative NAO-like conditions can be reconstructed for $2820^{+180}/_{-180}$-$2110^{+155}/_{-130}$ cal BP and $830^{+100}/_{-90}$-$105^{+95}/_{-75}$ cal BP.~~ Rates of changes between positive to negative conditions vary between the individual phases, e.g. with a rapid drop in winter temperature around $2820^{+180}/_{-180}$ cal BP but a gradual increase from $2110^{+155}/_{-130}$-$1720^{+65}/_{-65}$ cal BP. ~~After $105^{+95}/_{-75}$ cal BP.~~ After $105^{+95}/_{-75}$ cal BP, the anthropogenic impact on Schweriner See increased significantly, resulting in in-lake productivity
920 mainly driven by nutrient supply (eutrophication) ~~and~~masking the hydroclimatic signal.
In addition to these long-term shifts in atmospheric ~~conditions~~circulation systems, short-term hydroclimatic variations can be reconstructed. In this context, ~~titanium~~Ti mainly reflects lake-level variations linked to precipitation/evaporation variability with additional influences of wind speed ~~influences, resulting in increased~~strengthening wave action. This mode of minerogenic ~~input~~matter supply contradicts traditional interpretations and highlights the importance of carefully considering
925 lake morphology, catchment and environmental conditions for proxy interpretation.

Data availability

The original data from this study will be available upon request and in the PANGAEA repository.

930 **Author Contributions**

MLA – Conceptualization, Methodology, Formal analysis, Investigation, Visualization, Writing – original draft preparation, Writing – review and editing; SC – Investigation, Writing – review and editing; MDr – Investigation, Writing – review and editing; PS – Investigation, Writing – review and editing; MB – Investigation, Writing – review and editing; SL – Conceptualization, Funding acquisition, Writing – review and editing; MDe – Methodology, Resources; TH –
935 Conceptualization, Methodology, Funding acquisition, Writing – review and editing, Supervision

Funding

This project was funded by the German Research Foundation (HA5089/14-1) and was carried out in close cooperation with the Ministry for Climate Protection, Agriculture, Rural Areas and Environment Mecklenburg-Vorpommern.
940

Competing Interests

The contact author has declared that none of the authors has any competing interests

Acknowledgement

945 MLA received a Graduate Scholarship (Landesgraduiertenstipendium) from the Federal State of Mecklenburg-Western Pomerania to conduct this research. We want to acknowledge J. Becker and M. Steinich for their support of the field campaign and M. Steinich and U. Dolgner for CNS and TIC analyses. Moreover, we want to thank Kaja Müller, Antonia Kühn and Rafael Tüllinghoff for their support during sampling and laboratory analyses. We would also like to thank Peter Appleby for carrying out the [137]Cs- and ^{210}Pb dating and Christian Ohlendorf and Rafael Stiens for XRF scanning. We want to thank Roland
950 Zech for discussions and laboratory and instrument access at the Physical Geography department of the Friedrich -Schiller University Jena. Moreover, we thank Kevin Jacq for his support during the Hyperspectral Imaging.

References

Adolph, M.-L.: Late Holocene environmental variability derived from lacustrine sediments of large lowland lake Schweriner See, NE-Germany, PhD Thesis, Universität Greifswald, Greifswald, 2024.
955 Adolph, M.-L., Dreßler, M., Troelstra, V., Wrozyna, C., and Haberzettl, T.: Eutrophication and contamination dynamics of Schweriner See, NE-Germany, during the past 670 years – A multi-proxy approach on lacustrine surface sediments and sediment cores, Science of the Total Environment, 877, doi:10.1016/j.scitotenv.2023.162745, 2023.

Adolph, M.-L., Lampe, R., Lorenz, S., and Haberzettl, T.: Characterization of (paleo)lacustrine landforms using sedimentological and portable OSL investigations at Schweriner See, north-eastern Germany, Earth Surf. Process. Landforms, 42, 422–435, doi:10.1002/esp.5258, 2022.

Aichner, B., Dubbert, D., Kiel, C., Kohnert, K., Ogashawara, I., Jechow, A., Harpenslager, S.-F., Hölker, F., Nejstgaard, J. C., Grossart, H.-P., Singer, G., Wollrab, S., and Berger, S. A.: Spatial and seasonal patterns of water isotopes in northeastern German lakes, Earth Syst. Sci. Data, 14, 1857–1867, doi:10.5194/essd-14-1857-2022, 2022.

Aitchison, J.: The Statistical Analysis of Compositional Data, Journal of the Royal Statistical Society: Series B (Methodological), 44, 139–160, doi:10.1111/j.2517-6161.1982.tb01195.x, 1982.

Appleby, P. G., Nolan, P. J., Gifford, D. W., Godfrey, M. J., Oldfield, F., Anderson, N. J., and Battarbee, R. W.: [210]Pb dating by low background gamma counting, Hydrobiologia, 143, 21–27, doi:10.1007/BF00026640, 1986.

Appleby, P. G., Richardson, N., and Nolan, P. J.: Self-absorption corrections for well-type germanium detectors, Nuclear Instruments and Methods in Physics Research Section B: Beam Interactions with Materials and Atoms, 71, 228–233, doi:10.1016/0168-583X(92)95328-O, 1992.

Baker, A., C Hellstrom, J., Kelly, B. F. J., Mariethoz, G., and Trouet, V.: A composite annual-resolution stalagmite record of North Atlantic climate over the last three millennia, Scientific Reports, 5, 10307, doi:10.1038/srep10307, 2015.

Baldini, L. M., McDermott, F., Foley, A. M., and Baldini, J. U. L.: Spatial variability in the European winter precipitation δ^{18}O-NAO relationship: Implications for reconstructing NAO-mode climate variability in the Holocene, Geophys. Res. Lett., 35, doi:10.1029/2007GL032027, 2008.

Barber, K., Chambers, F., and Maddy, D.: Late Holocene climatic history of northern Germany and Denmark: peat macrofossil investigations at Dosenmoor, Schleswig-Holstein, and Svanemose, Jutland, Boreas, 33, 132–144, doi:10.1080/03009480410001082, 2004.

Becker, L. W. M., Sejrup, H. P., Hjelstuen, B. O., Haflidason, H., Kjennbakken, H., and Werner, J. P.: Palaeo-productivity record from Norwegian Sea enables North Atlantic Oscillation (NAO) reconstruction for the last 8000 years, npj Clim Atmos Sci, 3, 1–12, doi:10.1038/s41612-020-00147-6, 2020.

Berglund, B. and Ralska-Jasiewiczowa, M.: Pollen analysis and pollen diagrams, in: Handbook of Holocene Palaeoecology and Palaeohydrology, Berglund, B. (Ed.), John Wiley & Sons, Chichester, 455–484, 1986.

Beug, H. J.: Leitfaden der Pollenbestimmung für Mitteleuropa und angrenzende Gebiete., Verlag Friedrich Pfeil, München, 2004.

Björck, S. and Clemmensen, L. B.: Aeolian sediment in raised bog deposits, Halland, SW Sweden: a new proxy record of Holocene winter storminess variation in southern Scandinavia?, The Holocene, 14, 677–688, doi:10.1191/0959683604hl746rp, 2004.

Blaauw, M. and Christen, J. A.: Flexible paleoclimate age-depth models using an autoregressive gamma process, Bayesian Anal., 6, 457–474, doi:10.1214/ba/1339616472, 2011.

Blenckner, T., Adrian, R., Livingstone, D. M., Jennings, E., Weyhenmeyer, G. A., George, D. G., Jankowski, T., Järvinen, M., Aonghusa, C., Nõges, T., Straile, D., and Teubner, K.: Large-scale climatic signatures in lakes across Europe: a meta-analysis, Global Change Biol, 13, 1314–1326, doi:10.1111/j.1365-2486.2007.01364.x, 2007.

Bliedtner, M., Strobel, P., Struck, J., Prochnow, M., Bazarradnaa, E., and Zech, R.: Mid to Late Holocene moisture evolution of semi-arid Mongolia and its anti-phase relationship with monsoonal Asia, Quat. Sci. Rev., 313, 108201, doi:10.1016/j.quascirev.2023.108201, 2023.

Bliedtner, M., Zech, R., Zech, J., Schäfer, I., and Suchodoletz, H.: A first Holocene leaf wax isotope-based paleoclimate record from the semi-humid to semi-arid south-eastern Caucasian lowlands, J. Quaternary Sci, 35, 625–633, doi:10.1002/jqs.3210, 2020.

Blott, S. J. and Pye, K.: GRADISTAT: a grain size distribution and statistics package for the analysis of unconsolidated sediments, Earth Surf. Process. Landforms, 26, 1237–1248, doi:10.1002/esp.261, 2001.

Bond, G., Kromer, B., Beer, J., Muscheler, R., Evans, M. N., Showers, W., Hoffmann, S., Lotti-Bond, R., Hajdas, I., and Bonani, G.: Persistent solar influence on North Atlantic climate during the Holocene, Science, 294, 2130–2136, doi:10.1126/science.1065680, 2001.

Bonk, A., Piotrowska, N., Żarczyński, M., Enters, D., Makohonienko, M., Rzodkiewicz, M., and Tylmann, W.: Limnological responses to environmental changes during the last 3,000 years revealed from a varved sequence of Lake Lubińskie (western Poland), Catena, 226, 107053, doi:10.1016/j.catena.2023.107053, 2023.

Bonsal, B. R., Prowse, T. D., Duguay, C. R., and Lacroix, M. P.: Impacts of large-scale teleconnections on freshwater-ice break/freeze-up dates over Canada, Journal of Hydrology, 330, 340–353, doi:10.1016/j.jhydrol.2006.03.022, 2006.

Bradshaw, R., Kito, N., and Giesecke, T.: Factors influencing the Holocene history of Fagus, Forest Ecology and Management, 259, 2204–2212, doi:10.1016/j.foreco.2009.11.035, 2010.

Breitenbach, S. F., Plessen, B., Waltgenbach, S., Tjallingii, R., Leonhardt, J., Jochum, K. P., Meyer, H., Goswami, B., Marwan, N., and Scholz, D.: Holocene interaction of maritime and continental climate in Central Europe: New speleothem evidence from Central Germany, Global and Planetary Change, 176, 144–161, doi:10.1016/j.gloplacha.2019.03.007, 2019.

Büntgen, U., Urban, O., Krusic, P. J., Rybníček, M., Kolář, T., Kyncl, T., Ač, A., Koňasová, E., Čáslavský, J., Esper, J., Wagner, S., Saurer, M., Tegel, W., Dobrovolný, P., Cherubini, P., Reinig, F., and Trnka, M.: Recent European drought extremes beyond Common Era background variability, Nat. Geosci., 14, 190–196, doi:10.1038/s41561-021-00698-0, 2021.

Carmer, C. F. von: Gewässerkulturlandschaften - Die historische Dimension kleiner Fließgewässer am Beispiel des Wallensteingrabens, Wasserwirtschaft, 7-8, 28–32, 2006.

Charman, D. J., Barber, K. E., Blaauw, M., Langdon, P. G., Mauquoy, D., Daley, T. J., Hughes, P. D., and Karofeld, E.: Climate drivers for peatland palaeoclimate records, Quat. Sci. Rev., 28, 1811–1819, doi:10.1016/j.quascirev.2009.05.013, 2009.

1025 Comas-Bru, L. and McDermott, F.: Impacts of the EA and SCA patterns on the European twentieth century NAO-winter climate relationship, Q.J.R. Meteorol. Soc., 140, 354–363, doi:10.1002/qj.2158, 2014.

Comas-Bru, L., McDermott, F., and Werner, M.: The effect of the East Atlantic pattern on the precipitation δ^{18}O-NAO relationship in Europe, Clim Dyn, 47, 2059–2069, doi:10.1007/s00382-015-2950-1, 2016.

Croudace, I. W. and Rothwell, G.: Micro-XRF sediment core scanners: important new tools for the environmental and earth

1030 sciences, Spectroscopy Europe, 3, 6–13, 2010.

Czymzik, M., Tjallingii, R., Plessen, B., Feldens, P., Theuerkauf, M., Moros, M., Schwab, M. J., Nantke, C. K. M., Pinkerneil, S., Brauer, A., and Arz, H. W.: Mid-Holocene reinforcement of North Atlantic atmospheric circulation variability from a western Baltic lake sediment record, Clim. Past, 19, 233–248, doi:10.5194/cp-19-233-2023, 2023.

Daley, T. J. and Barber, K. E.: Multi-proxy Holocene palaeoclimate records from Walton Moss, northern England and

1035 Dosenmoor, northern Germany, assessed using three statistical approaches, Quaternary International, 268, 111–127, doi:10.1016/j.quaint.2011.10.026, 2012.

Davies, S. J., Lamb, H. F., and Roberts, S. J.: Micro-XRF Core Scanning in Palaeolimnology: Recent Developments, in: Micro-XRF Studies of Sediment Cores: Applications of a non-destructive tool for the environmental sciences, Croudace, I. W., Rothwell, R. G. (Eds.), Springer Netherlands, Dordrecht, 189–226, 2015.

1040 Debret, M., Sebag, D., Desmet, M., Balsam, W. L., Copard, Y., Mourier, B., Susperrigui, A.-S., Arnaud, F., Bentaleb, I., Chapron, E., Lallier-Vergès, E., and Winiarski, T.: Spectrocolorimetric interpretation of sedimentary dynamics: The new "Q7/4 diagram", Earth-Science Reviews, 109, 1–19, doi:10.1016/j.earscirev.2011.07.002, 2011.

Dietze, E., Słowiński, M., Zawiska, I., Veh, G., and Brauer, A.: Multiple drivers of Holocene lake level changes at a lowland lake in northeastern Germany, Boreas, 45, 828–845, doi:10.1111/bor.12190, 2016.

1045 Doberschütz, S., Frenzel, P., Haberzettl, T., Kasper, T., Wang, J., Zhu, L., Daut, G., Schwalb, A., and Mäusbacher, R.: Monsoonal forcing of Holocene paleoenvironmental change on the central Tibetan Plateau inferred using a sediment record from Lake Nam Co (Xizang, China), J Paleolimnol, 51, 253–266, doi:10.1007/s10933-013-9702-1, 2014.

Dräger, N., Theuerkauf, M., Szeroczyńska, K., Wulf, S., Tjallingii, R., Plessen, B., Kienel, U., and Brauer, A.: Varve microfacies and varve preservation record of climate change and human impact for the last 6000 years at Lake Tiefer

1050 See (NE Germany), The Holocene, 27, 450–464, doi:10.1177/0959683616660173, 2017.

Dreßler, M., Schwarz, A., Hübener, T., Adler, S., and Scharf, B. W.: Use of sedimentary diatoms from multiple lakes to distinguish between past changes in trophic state and climate: evidence for climate change in northern Germany during the past 5,000 years, J Paleolimnol, 45, 223–241, doi:10.1007/s10933-010-9494-5, 2011.

DWD Climate Data Center: Multi-annual grids of water balance over Germany 1971-2000, Deutscher Wetterdienst, 2020.

1055 DWD Climate Data Center: Hourly mean of station observations of wind direction ca. 10 m above ground in degree for Germany: Weather Station Schwerin, Deutscher Wetterdienst, 2022a.

DWD Climate Data Center: Monthly mean of station observations of air temperature at 2 m above ground in °C for Schwerin, Deutscher Wetterdienst, 2022b.

DWD Climate Data Center: Monthly station observations of precipitation in mm for Schwerin, Deutscher Wetterdienst,
1060   2022c.

Engels, S., Bakker, M. A., Bohncke, S. J., Cerli, C., Hoek, W. Z., Jansen, B., Peters, T., Renssen, H., Sachse, D., van Aken, J. M., van den Bos, V., van Geel, B., van Oostrom, R., Winkels, T., and Wolma, M.: Centennial-scale lake-level lowstand at Lake Uddelermeer (The Netherlands) indicates changes in moisture source region prior to the 2.8-kyr event, The Holocene, 26, 1075–1091, doi:10.1177/0959683616632890, 2016.

1065   Faust, J. C., Fabian, K., Milzer, G., Giraudeau, J., and Knies, J.: Norwegian fjord sediments reveal NAO related winter temperature and precipitation changes of the past 2800 years, Earth and Planetary Science Letters, 435, 84–93, doi:10.1016/j.epsl.2015.12.003, 2016.

Feakins, S. J. and Sessions, A. L.: Controls on the D/H ratios of plant leaf waxes in an arid ecosystem, Geochimica et Cosmochimica Acta, 74, 2128–2141, doi:10.1016/j.gca.2010.01.016, 2010.

1070   Fellner, B.: Faszination Lewitz: Ein Naturparadies in Mecklenburg, 2nd ed., Fellner, Neustadt-Glewe, 144 pp., 2007.

Ficken, K., Li, B., Swain, D., and Eglinton, G.: An n-alkane proxy for the sedimentary input of submerged/floating freshwater aquatic macrophytes, Organic Geochemistry, 31, 745–749, doi:10.1016/S0146-6380(00)00081-4, 2000.

Giesecke, T., Brewer, S., Finsinger, W., Leydet, M., and Bradshaw, R. H.: Patterns and dynamics of European vegetation change over the last 15,000 years, J. Biogeogr., 44, 1441–1456, doi:10.1111/jbi.12974, 2017.

1075   Goslin, J., Fruergaard, M., Sander, L., Gałka, M., Menviel, L., Monkenbusch, J., Thibault, N., and Clemmensen, L. B.: Holocene centennial to millennial shifts in North-Atlantic storminess and ocean dynamics, Sci Rep, 8, 12778, doi:10.1038/s41598-018-29949-8, 2018.

Gray, L. J., Woollings, T. J., Andrews, M., and Knight, J.: Eleven-year solar cycle signal in the NAO and Atlantic/European blocking, Q.J.R. Meteorol. Soc., 142, 1890–1903, doi:10.1002/qj.2782, 2016.

1080   Günther, F., Thiele, A., Biskop, S., Mäusbacher, R., Haberzettl, T., Yao, T., and Gleixner, G.: Late quaternary hydrological changes at Tangra Yumco, Tibetan Plateau: a compound-specific isotope-based quantification of lake level changes, J Paleolimnol, 55, 369–382, doi:10.1007/s10933-016-9887-1, 2016.

Haberzettl, T., Anselmetti, F. S., Bowen, S. W., Fey, M., Mayr, C., Zolitschka, B., Ariztegui, D., Mauz, B., Ohlendorf, C., Kastner, S., Lücke, A., Schäbitz, F., and Wille, M.: Late Pleistocene dust deposition in the Patagonian steppe - extending
1085   and refining the paleoenvironmental and tephrochronological record from Laguna Potrok Aike back to 55 ka, Quat. Sci. Rev., 28, 2927–2939, doi:10.1016/j.quascirev.2009.07.021, 2009.

Haberzettl, T., Corbella, H., Fey, M., Janssen, S., Lücke, A., Mayr, C., Ohlendorf, C., Schäbitz, F., Schleser, G. H., Wille, M., Wulf, S., and Zolitschka, B.: Lateglacial and Holocene wet—dry cycles in southern Patagonia: chronology, sedimentology and geochemistry of a lacustrine record from Laguna Potrok Aike, Argentina, The Holocene, 17, 297–
1090   310, doi:10.1177/0959683607076437, 2007.

Haberzettl, T., Fey, M., Lücke, A., Maidana, N., Mayr, C., Ohlendorf, C., Schäbitz, F., Schleser, G. H., Wille, M., and Zolitschka, B.: Climatically induced lake level changes during the last two millennia as reflected in sediments of Laguna

Potrok Aike, southern Patagonia (Santa Cruz, Argentina), J Paleolimnol, 33, 283–302, doi:10.1007/s10933-004-5331-z, 2005.

1095   Haberzettl, T., Kirsten, K. L., Kasper, T., Franz, S., Reinwarth, B., Baade, J., Daut, G., Meadows, M. E., Su, Y., and Mäusbacher, R.: Using ^{210}Pb-data and paleomagnetic secular variations to date anthropogenic impact on a lake system in the Western Cape, South Africa, Quaternary Geochronology, 51, 53–63, doi:10.1016/j.quageo.2018.12.004, 2019.

Hammer, Ø.: PAST: PAleontological STatistics, Oslo, 2022.

Harding, P., Martin-Puertas, C., Sjolte, J., Walsh, A. A., Tjallingii, R., Langdon, C., Blockley, S. P. E., Brauer, A., Langdon,
1100   P., Milner, A. M., Muscheler, R., and Perez, M.: Wind regime changes in the Euro-Atlantic region driven by Late-Holocene Grand Solar Minima, Clim Dyn, 60, 1947–1961, doi:10.1007/s00382-022-06388-w, 2023.

Harrell Jr, F. E.: Hmisc: Harrell Miscellaneous: R-package, 2023.

Hodell, D. A., Channell, J. E. T., Curtis, J. H., Romero, O. E., and Röhl, U.: Onset of "Hudson Strait" Heinrich events in the eastern North Atlantic at the end of the middle Pleistocene transition (~640 ka)?, Paleoceanography, 23, 1-16,
1105   doi:10.1029/2008PA001591, 2008.

Hodell, D. A. and Schelske, C. L.: Production, sedimentation, and isotopic composition of organic matter in Lake Ontario, Limnol. Oceanogr., 43, 200–214, doi:10.4319/lo.1998.43.2.0200, 1998.

Hu, H.-M., Trouet, V., Spötl, C., Tsai, H.-C., Chien, W.-Y., Sung, W.-H., Michel, V., Yu, J.-Y., Valensi, P., Jiang, X., Duan, F., Wang, Y., Mii, H.-S., Chou, Y.-M., Lone, M. A., Wu, C.-C., Starnini, E., Zunino, M., Watanabe, T. K., Watanabe,
1110   T., Hsu, H.-H., Moore, G. W. K., Zanchetta, G., Pérez-Mejías, C., Lee, S.-Y., and Shen, C.-C.: Tracking westerly wind directions over Europe since the middle Holocene, Nature Communications, 13, 7866, doi:10.1038/s41467-022-34952-9, 2022.

Hurrell, J. W.: Decadal Trends in the North Atlantic Oscillation: Regional Temperatures and Precipitation, Science, 269, 676–679, doi:10.1126/science.269.5224.676, 1995.

1115   Hurrell, J. W. (Ed.): The North Atlantic oscillation: Climatic significance and environmental impact, Geophysical Monograph Series, 134, American Geophysical Union, Washington, D.C., 279 pp., 2003.

Hurrell, J. W. and Deser, C.: North Atlantic climate variability: The role of the North Atlantic Oscillation, Journal of Marine Systems, 78, 28–41, doi:10.1016/j.jmarsys.2008.11.026, 2009.

Hurrell, J. W., Kushnir, Y., Ottersen, G., and Visbeck, M.: An overview of the North Atlantic Oscillation, in: The North
1120   Atlantic oscillation: Climatic significance and environmental impact, Hurrell, J. W. (Ed.), Geophysical Monograph Series, 134, American Geophysical Union, Washington, D.C., 1–35, 2003.

IPCC: Climate Change 2021: The Physical Science Basis: Contribution of Working Group I to the Sixth Assessment Report of the Intergovernmental Panel on Climate Change, Cambridge Univ. Press, Cambridge, New York, 2409 pp., 2021.

Jacq, K., Auboiron, J., Humbert, K., Martinez-Lamas, R., van Exem, A., and Debret, M.: Hyperspectral core-logger image
1125   acquisition v.2, Berkeley, CA, USA, 2021.

Jong, R. de, Björck, S., Björkman, L., and Clemmensen, L. B.: Storminess variation during the last 6500 years as reconstructed from an ombrotrophic peat bog in Halland, southwest Sweden, J. Quaternary Sci, 21, 905–919, doi:10.1002/jqs.1011, 2006.

Jong, R. de, Schoning, K., and Björck, S.: Increased aeolian activity during humidity shifts as recorded in a raised bog in south-west Sweden during the past 1700 years, Clim. Past, 3, 411–422, doi:10.5194/cp-3-411-2007, 2007.

Juggins, S.: rioja: Analysis of Quaternary Science Data, R package, 2022.

Kahmen, A., Hoffmann, B., Schefuß, E., Arndt, S. K., Cernusak, L. A., West, J. B., and Sachse, D.: Leaf water deuterium enrichment shapes leaf wax n-alkane δD values of angiosperm plants II: Observational evidence and global implications, Geochimica et Cosmochimica Acta, 111, 50–63, doi:10.1016/j.gca.2012.09.004, 2013.

Kaiser, K., Lorenz, S., Germer, S., Juschus, O., Küster, M., Libra, J., Bens, O., and Hüttl, R. F.: Late Quaternary evolution of rivers, lakes and peatlands in northeast Germany reflecting past climatic and human impact - an overview, E&G Quaternary Sci. J., 61, 103–132, doi:10.3285/eg.61.2.01, 2012.

Kalbe, L. and Werner, H.: Das Sediment des Kummerower Sees. Untersuchungen des Chemismus und der Diatomeenflora, Int. Revue ges. Hydrobiol. Hydrogr., 59, 755–782, doi:10.1002/iroh.19740590603, 1974.

Kasper, T., Frenzel, P., Haberzettl, T., Schwarz, A., Daut, G., Meschner, S., Wang, J., Zhu, L., and Mäusbacher, R.: Interplay between redox conditions and hydrological changes in sediments from Lake Nam Co (Tibetan Plateau) during the past 4000cal BP inferred from geochemical and micropaleontological analyses, Palaeogeography, Palaeoclimatology, Palaeoecology, 392, 261–271, doi:10.1016/j.palaeo.2013.09.027, 2013.

Kasper, T., Haberzettl, T., Doberschütz, S., Daut, G., Wang, J., Zhu, L., Nowaczyk, N., and Mäusbacher, R.: Indian Ocean Summer Monsoon (IOSM)-dynamics within the past 4 ka recorded in the sediments of Lake Nam Co, central Tibetan Plateau (China), Quat. Sci. Rev., 39, 73–85, doi:10.1016/j.quascirev.2012.02.011, 2012.

Kasten, B. and Rost, J.-U.: Schwerin: Geschichte der Stadt, Helms, Schwerin, 400 pp., 2005.

Konze, M.: Bergung und Dokumentation von Teilen des Bodendenkmals „Schloss Schwerin" (Fpl. 17) im Rahmen des Projektes „Schloss Schwerin, Ver- und Entsorgungsleitungen im Innenhof" (3544-4098-HS), Landesamt für Kultur und Denkmalpflege Mecklenburg-Vorpommern, Schwerin, 2017.

Krammer, K.: Die cymbelloiden Diatomeen: Eine Monographie der weltweit bekannten Taxa, Bibliotheca diatomologica, 36, Cramer, Berlin, 382 pp., 1997a.

Krammer, K.: Die cymbelloiden Diatomeen: Eine Monographie der weltweit bekannten Taxa, Bibliotheca diatomologica, 37, Cramer, Berlin, 469 pp., 1997b.

Krammer, K.: The genus Pinnularia, Diatoms of Europe, 1, Gantner; Koeltz, Ruggell/Liechtenstein, Königstein/Germany, 703 pp., 2000.

Krammer, K.: Cymbella, Diatoms of Europe, 3, Gantner; Koeltz, Ruggell/Liechtenstein, Königstein/Germany, 584 pp., 2002.

Krammer, K.: Cymbopleura, Delicata, Navicymbula, Gomphocymbellopsis, Afrocymbella, Diatoms of Europe, 4, Gantner;
1160   Koeltz, Ruggell/Liechtenstein, Königstein/Germany, 530 pp., 2003.

Krammer, K. and Lange-Bertalot, H.: Naviculaceae, Süßwasserflora von Mitteleuropa, 2.1, G. Fischer, Stuttgart, 876 pp.,
1986.

Krammer, K. and Lange-Bertalot, H.: Bacillariophyceae, Süßwasserflora von Mitteleuropa, 2.2, G. Fischer, Stuttgart, 596
pp., 1988.

1165   Krammer, K. and Lange-Bertalot, H.: Achnanthaceae, Kritische Ergänzungen zu Navicula (Lineolatae) und Gomphonema,
Gesamtliteraturverzeichnis Teil 1 - 4: 88 Tafeln mit 2048 Figuren, Süßwasserflora von Mitteleuropa, 2.4, G. Fischer,
Stuttgart, 437 pp., 1991a.

Krammer, K. and Lange-Bertalot, H.: Centrales, Fragilariaceae, Eunotiaceae, Süßwasserflora von Mitteleuropa, 2.3, G.
Fischer, Stuttgart, 576 pp., 1991b.

1170   Krienke, H.-D. and Obst, K.: Raben Steinfeld und die Eiszeit - Landschaftsentwicklung und geologische
Sehenswürdigkeiten südöstlich von Schwerin, Brandenburgische geowissenschaftliche Beiträge, 18, 107–123, 2011.

Kylander, M. E., Ampel, L., Wohlfarth, B., and Veres, D.: High-resolution X-ray fluorescence core scanning analysis of Les
Echets (France) sedimentary sequence: new insights from chemical proxies, J. Quaternary Sci, 26, 109–117,
doi:10.1002/jqs.1438, 2011.

1175   Lamb, H. H.: Climate: Present, Past and Future: Volume 2: Climatic History and the Future, Routledge Revivals, Taylor and
Francis, Hoboken, 879 pp., 2013.

Lampe, M. and Lampe, R.: Evolution of a large Baltic beach ridge plain (Neudarss, NE Germany): A continuous record of
sea-level and wind-field variation since the Homeric Minimum, Earth Surf. Process. Landforms, 43, 3042–3056,
doi:10.1002/esp.4468, 2018.

1180   Lampe, R., Lorenz, S., Janke, W., Meyer, H., Küster, M., Hübener, T., and Schwarz, A.: Zur Landschafts- und
Gewässergeschichte der Müritz: Umweltgeschichtlich orientierte Bohrungen 2004 - 2006 zur Rekonstruktion der
nacheiszeitlichen Entwicklung, 1. Aufl., Forschung und Monitoring, 2, Geozon Science Media, Greifswald, 93 pp.,
2009.

Landesamt für Umwelt, Naturschutz und Geologie Mecklenburg-Vorpommern (Ed.): Hydrologisches Jahr 2018: Bericht zur
1185   hydrometeorologischen und hydrologischen Lage in Mecklenburg Vorpommern, 01.11.2017 bis 31.10.2018, Landesamt
für Umwelt, Naturschutz und Geologie Mecklenburg-Vorpommern, Güstrow, 28 pp., 2018.

Lange-Bertalot, H.: Navicula sensu stricto, 10 genera separated from Navicula sensu lato, Frustulia, Diatoms of Europe, Vol.
2, Gantner; Koeltz Gantner, Ruggell/Liechtenstein, Königstein/Germany, Ruggell, 526 pp., 2001.

Lange-Bertalot, H., Bąk, M., and Witkowski, A.: Eunotia and some related genera, Diatoms of Europe, Vol. 6, Gantner;
1190   Koeltz, Ruggell/Liechtenstein, Königstein/Germany, 747 pp., 2011.

Lange-Bertalot, H., Cantonati, M., Kelly, M. G., Gabriele, H., and Marcus, W. (Eds.): Freshwater benthic diatoms of Central Europe: Over 800 common species used in ecological assessment, English edition with updated taxonomy and added species, Koeltz Botanical Books, Schmitten-Oberreifenberg, 942 pp., 2017.

Lorenz, S.: Die spätpleistozäne und holozäne Gewässernetzentwicklung im Bereich der Pommerschen Haupteisrandlage Mecklenburgs, Dissertation, Universität Greifswald, Greifswald, 351 pp., 2007.

Lorenz, S., Adolph, M.-L., Schult, M., Černý, A., and Besler, C.: Der Schweriner See - ein Blick in die Landschaftsgeschichte, in: Zvarin - Schwerin: Von der Inselburg zur Residenz, Ruchhöft, F. (Ed.), Landesamt für Kultur und Denkmalpflege Mecklenburg-Vorpommern, Schwerin, 129–141, 2017.

Magny, M.: Holocene climate variability as reflected by mid-European lake-level fluctuations and its probable impact on prehistoric human settlements, Quaternary International, 113, 65–79, doi:10.1016/s1040-6182(03)00080-6, 2004.

Martínez Cortizas, A., Sjöström, J. K., Ryberg, E. E., Kylander, M. E., Kaal, J., López-Costas, O., Álvarez Fernández, N., and Bindler, R.: 9000 years of changes in peat organic matter composition in Store Mosse (Sweden) traced using FTIR-ATR, Boreas, 50, 1161–1178, doi:10.1111/bor.12527, 2021.

Martin-Puertas, C., Matthes, K., Brauer, A., Muscheler, R., Hansen, F., Petrick, C., Aldahan, A., Possnert, G., and van Geel, B.: Regional atmospheric circulation shifts induced by a grand solar minimum, Nat. Geosci., 5, 397–401, doi:10.1038/ngeo1460, 2012.

McDermott, F., Atkinson, T. C., Fairchild, I. J., Baldini, L. M., and Mattey, D. P.: A first evaluation of the spatial gradients in δ^{18}O recorded by European Holocene speleothems, Global and Planetary Change, 79, 275–287, doi:10.1016/j.gloplacha.2011.01.005, 2011.

Meinke, I., Rechid, D., Tinz, B., Maneke, M., Lefebvre, C., and Isokeit, E.: Klima der Region – Zustand, bisherige Entwicklung und mögliche Änderungen bis 2100, in: Hamburger Klimabericht - Wissen über Klima, Klimawandel und Auswirkungen in Hamburg und Norddeutschland, Storch, H. von, Meinke, I., Claussen, M. (Eds.), Springer eBook Collection, Springer Spektrum, Berlin, Heidelberg, 15–36, 2018.

Mellado-Cano, J., Barriopedro, D., García-Herrera, R., Trigo, R. M., and Hernández, A.: Examining the North Atlantic Oscillation, East Atlantic Pattern, and Jet Variability since 1685, Journal of Climate, 32, 6285–6298, doi:10.1175/JCLI-D-19-0135.1, 2019.

Mellström, A., van der Putten, N., Muscheler, R., Jong, R. de, and Björck, S.: A shift towards wetter and windier conditions in southern Sweden around the prominent solar minimum 2750 cal a BP, J. Quaternary Sci, 30, 235–244, doi:10.1002/jqs.2776, 2015.

Meyers, P. A. and Ishiwatari, R.: Lacustrine organic geochemistry—an overview of indicators of organic matter sources and diagenesis in lake sediments, Organic Geochemistry, 20, 867–900, doi:10.1016/0146-6380(93)90100-p, 1993.

Moffa-Sánchez, P., Born, A., Hall, I. R., Thornalley, D. J. R., and Barker, S.: Solar forcing of North Atlantic surface temperature and salinity over the past millennium, Nat. Geosci., 7, 275–278, doi:10.1038/ngeo2094, 2014.

Moore, G. W. K., Pickart, R. S., and Renfrew, I. A.: Complexities in the climate of the subpolar North Atlantic: a case study from the winter of 2007, Q.J.R. Meteorol. Soc., 137, 757–767, doi:10.1002/qj.778, 2011.

Moore, G. W. K. and Renfrew, I. A.: Cold European winters: interplay between the NAO and the East Atlantic mode, Atmosph. Sci. Lett., 13, 1–8, doi:10.1002/asl.356, 2012.

Moore, G. W. K., Renfrew, I. A., and Pickart, R. S.: Multidecadal Mobility of the North Atlantic Oscillation, Journal of Climate, 26, 2453–2466, doi:10.1175/JCLI-D-12-00023.1, 2013.

Moore, P. D., Webb, J. A., and Collinson, M. E.: Pollen analysis, 2nd ed., Blackwell Scientific Publications, Oxford, 216 pp., 1991.

Mügler, I., Sachse, D., Werner, M., Xu, B., Wu, G., Yao, T., and Gleixner, G.: Effect of lake evaporation on δD values of lacustrine n-alkanes: A comparison of Nam Co (Tibetan Plateau) and Holzmaar (Germany), Organic Geochemistry, 39, 711–729, doi:10.1016/j.orggeochem.2008.02.008, 2008.

Nakagawa, T.: High-precision sampling of laminated sediments: Strategies from Lake Suigetsu, PAGES Mag, 22, 12–13, doi:10.22498/pages.22.1.12, 2014.

Nixdorf, B., Hemm, M., Hoffmann, A., and Richter, P.: Dokumentation von Zustand und Entwicklung der wichtigsten Seen Deutschlands: Teil 2 - Mecklenburg-Vorpommern, Brandenburgische Technische Universität Cottbus, Berlin, 2004.

Olsen, J., Anderson, N. J., and Knudsen, M. F.: Variability of the North Atlantic Oscillation over the past 5,200 years, Nat. Geosci., 5, 808–812, doi:10.1038/ngeo1589, 2012.

PAGES 2k Consortium: Continental-scale temperature variability during the past two millennia, Nat. Geosci., 6, 339–346, doi:10.1038/ngeo1797, 2013.

Pedersen, T. L., Nicolae, B., and Francios, R.: farver: High Performance Colour Space Manipulation, 2022.

Pleskot, K., Tjallingii, R., Makohonienko, M., Nowaczyk, N., and Szczuciński, W.: Holocene paleohydrological reconstruction of Lake Strzeszyńskie (western Poland) and its implications for the central European climatic transition zone, J Paleolimnol, 59, 443–459, doi:10.1007/s10933-017-9999-2, 2018.

Pouzet, P., Maanan, M., Piotrowska, N., Baltzer, A., Stéphan, P., and Robin, M.: Chronology of Holocene storm events along the European Atlantic coast, Progress in Physical Geography: Earth and Environment, 42, 431–450, doi:10.1177/0309133318776500, 2018.

Rach, O., Engels, S., Kahmen, A., Brauer, A., Martín-Puertas, C., van Geel, B., and Sachse, D.: Hydrological and ecological changes in western Europe between 3200 and 2000 years BP derived from lipid biomarker δD values in lake Meerfelder Maar sediments, Quat. Sci. Rev., 172, 44–54, doi:10.1016/j.quascirev.2017.07.019, 2017.

Reimer, P. J., Austin, W. E. N., Bard, E., Bayliss, A., Blackwell, P. G., Bronk Ramsey, C., Butzin, M., Cheng, H., Edwards, R. L., Friedrich, M., Grootes, P. M., Guilderson, T. P., Hajdas, I., Heaton, T. J., Hogg, A. G., Hughen, K. A., Kromer, B., Manning, S. W., Muscheler, R., Palmer, J. G., Pearson, C., van der Plicht, J., Reimer, R. W., Richards, D. A., Scott, E. M., Southon, J. R., Turney, C. S. M., Wacker, L., Adolphi, F., Büntgen, U., Capano, M., Fahrni, S. M., Fogtmann-Schulz, A., Friedrich, R., Köhler, P., Kudsk, S., Miyake, F., Olsen, J., Reinig, F., Sakamoto, M., Sookdeo, A., and

Talamo, S.: The IntCal20 Northern Hemisphere Radiocarbon Age Calibration Curve (0-55 cal kBP), Radiocarbon, 62(4), 725–757, doi:10.1017/RDC.2020.41, 2020.

1260 Ruchhöft, F. (Ed.): Zvarin - Schwerin: Von der Inselburg zur Residenz, Landesamt für Kultur und Denkmalpflege Mecklenburg-Vorpommern, Schwerin, 428 pp., 2017.

Sachse, D., Billault, I., Bowen, G. J., Chikaraishi, Y., Dawson, T. E., Feakins, S. J., Freeman, K. H., Magill, C. R., McInerney, F. A., van der Meer, M. T., Polissar, P., Robins, R. J., Sachs, J. P., Schmidt, H.-L., Sessions, A. L., White, J. W., West, J. B., and Kahmen, A.: Molecular Paleohydrology: Interpreting the Hydrogen-Isotopic Composition of Lipid

1265 Biomarkers from Photosynthesizing Organisms, Annu. Rev. Earth Planet. Sci., 40, 221–249, doi:10.1146/annurev-earth-042711-105535, 2012.

Sachse, D., Radke, J., and Gleixner, G.: Hydrogen isotope ratios of recent lacustrine sedimentary n-alkanes record modern climate variability, Geochimica et Cosmochimica Acta, 68, 4877–4889, doi:10.1016/j.gca.2004.06.004, 2004.

Scheffler, W. and Padisák, J.: Stephanocostis chantaicus (Bacillariophyceae): morphology and population dynamics of a rare

1270 centric diatom growing in winter under ice in the oligotrophic Lake Stechlin, Germany, Algological Studies, 98, 49–69, 2000.

Schmidt, D. F., Grise, K. M., and Pace, M. L.: High-frequency climate oscillations drive ice-off variability for Northern Hemisphere lakes and rivers, Climatic Change, 152, 517–532, doi:10.1007/s10584-018-2361-5, 2019.

Seierstad, I. A., Stephenson, D. B., and Kvamstø, N. G.: How useful are teleconnection patterns for explaining variability in

1275 extratropical storminess?, Tellus A: Dynamic Meteorology and Oceanography, 59, 170, doi:10.1111/j.1600-0870.2007.00226.x, 2007.

Shindell, D. T., Schmidt, G. A., Mann, M. E., Rind, D., and Waple, A.: Solar forcing of regional climate change during the Maunder Minimum, Science, 294, 2149–2152, doi:10.1126/science.1064363, 2001.

Shumilovskikh, L. S., Shumilovskikh, E. S., Schlütz, F., and van Geel, B.: NPP-ID: Non-Pollen Palynomorph Image

1280 Database as a research and educational platform, Veget Hist Archaeobot, 31, 323–328, doi:10.1007/s00334-021-00849-8, 2022.

Sjolte, J., Sturm, C., Adolphi, F., Vinther, B. M., Werner, M., Lohmann, G., and Muscheler, R.: Solar and volcanic forcing of North Atlantic climate inferred from a process-based reconstruction, Clim. Past, 14, 1179–1194, doi:10.5194/cp-14-1179-2018, 2018.

1285 Sorrel, P., Debret, M., Billeaud, I., Jaccard, S. L., McManus, J. F., and Tessier, B.: Persistent non-solar forcing of Holocene storm dynamics in coastal sedimentary archives, Nat. Geosci., 5, 892–896, doi:10.1038/ngeo1619, 2012.

Spinoni, J., Vogt, J. V., Naumann, G., Barbosa, P., and Dosio, A.: Will drought events become more frequent and severe in Europe?, Int. J. Climatol, 38, 1718–1736, doi:10.1002/joc.5291, 2018.

St. Amour, N. A., Hammerlund, D., Edwards, T., and Wolfe, B. B.: New insights into Holocene atmospheric circulation

1290 dynamics in central Scandinavia inferred from oxygen-isotope records of lake-sediment cellulose, Boreas, 39, 770–782, doi:10.1111/j.1502-3885.2010.00169.x, 2010.

Starkel, L., Michczyńska, D., Krąpiec, M., Margielewski, W., Nalepka, D., and Pazdur, A.: Progress in the Holocene chrono-climatostratigraphy of Polish territory, Geochronometria, 40, 1–21, doi:10.2478/s13386-012-0024-2, 2013.

Stockmarr, J.: Tablets with spores used in absolute pollen analysis, Pollen et spores, 13, 615–621, 1971.

1295   Strobel, P., Bliedtner, M., Carr, A. S., Struck, J., Du Plessis, N., Glaser, B., Meadows, M. E., Quick, L. J., Zech, M., Zech, R., and Haberzettl, T.: Reconstructing Late Quaternary precipitation and its source on the southern Cape coast of South Africa: A multi-proxy paleoenvironmental record from Vankervelsvlei, Quat. Sci. Rev., 284, 107467, doi:10.1016/j.quascirev.2022.107467, 2022a.

Strobel, P., Haberzettl, T., Bliedtner, M., Struck, J., Glaser, B., Zech, M., and Zech, R.: The potential of δ^2H$_{n\text{-alkanes}}$ and
1300 δ^{18}O$_{sugar}$ for paleoclimate reconstruction - A regional calibration study for South Africa, Science of the Total Environment, 716, 137045, doi:10.1016/j.scitotenv.2020.137045, 2020.

Strobel, P., Struck, J., Bazarradnaa, E., Zech, M., Zech, R., and Bliedtner, M.: Precipitation and Lake Water Evaporation Recorded by Terrestrial and Aquatic n-Alkane δ^2H Isotopes in Lake Khar Nuur, Mongolia, Geochem. Geophys. Geosyst., 23, doi:10.1029/2021GC010234, 2022b.

1305   Strobel, P., Struck, J., Zech, R., and Bliedtner, M.: The spatial distribution of sedimentary compounds and their environmental implications in surface sediments of Lake Khar Nuur (Mongolian Altai), Earth Surf. Process. Landforms, 46, 611–625, doi:10.1002/esp.5049, 2021.

Swindles, G. T., Plunkett, G., and Roe, H. M.: A delayed climatic response to solar forcing at 2800 cal. BP: multiproxy evidence from three Irish peatlands, The Holocene, 17, 177–182, doi:10.1177/0959683607075830, 2007.

1310   Theuerkauf, M., Blume, T., Brauer, A., Dräger, N., Feldens, P., Kaiser, K., Kappler, C., Kästner, F., Lorenz, S., Schmidt, J.-P., and Schult, M.: Holocene lake-level evolution of Lake Tiefer See, NE Germany, caused by climate and land cover changes, Boreas, 51, 299–316, doi:10.1111/bor.12561, 2022.

Trouet, V., Scourse, J. D., and Raible, C. C.: North Atlantic storminess and Atlantic Meridional Overturning Circulation during the last Millennium: Reconciling contradictory proxy records of NAO variability, Global and Planetary Change,
1315   84-85, 48–55, doi:10.1016/j.gloplacha.2011.10.003, 2012.

Umweltministerium Mecklenburg-Vorpommern (Ed.): Die Naturschutzgebiete in Mecklenburg-Vorpommern, Demmler, Schwerin, 713 pp., 2003.

Usoskin, I. G., Solanki, S. K., and Kovaltsov, G. A.: Grand minima and maxima of solar activity: new observational constraints, A&A, 471, 301–309, doi:10.1051/0004-6361:20077704, 2007.

1320   van Exem, A., Debret, M., Copard, Y., Jacq, K., Verpoorter, C., Marcotte, S., Laignel, B., and Vannière, B.: Hyperspectral Core-Logging for Past Primary Productivity Assessment, Quaternary, 5, 53, doi:10.3390/quat5040053, 2022.

van Geel, B., Heijnis, H., Charman, D. J., Thompson, G., and Engels, S.: Bog burst in the eastern Netherlands triggered by the 2.8 kyr BP climate event, The Holocene, 24, 1465–1477, doi:10.1177/0959683614544066, 2014.

van Geel, B., Heusser, C. J., Renssen, H., and Schuurmans, C. J.: Climatic change in Chile at around 2700 BP and global
1325   evidence for solar forcing: a hypothesis, The Holocene, 10, 659–664, doi:10.1191/09596830094908, 2000.

Vassiljev, J.: The simulated response of lakes to changes in annual and seasonal precipitation: implication for Holocene lake-level changes in northern Europe, Climate Dynamics, 14, 791–801, 1998.

Waltgenbach, S., Riechelmann, D. F. C., Spötl, C., Jochum, K. P., Fohlmeister, J., Schröder-Ritzrau, A., and Scholz, D.: Climate Variability in Central Europe during the Last 2500 Years Reconstructed from Four High-Resolution Multi-Proxy Speleothem Records, Geosciences, 11, 166, doi:10.3390/geosciences11040166, 2021.

Weltje, G. J. and Tjallingii, R.: Calibration of XRF core scanners for quantitative geochemical logging of sediment cores: Theory and application, Earth and Planetary Science Letters, 274, 423–438, doi:10.1016/j.epsl.2008.07.054, 2008.

Wiebeking, C. F. v.: Wiebekingsche Karte von Mecklenburg um 1786, Böhlau Verlag, Köln Wien, 1786.

Wirth, S. B. and Sessions, A. L.: Plant-wax D/H ratios in the southern European Alps record multiple aspects of climate variability, Quat. Sci. Rev., 148, 176–191, doi:10.1016/j.quascirev.2016.07.020, 2016.

Wöbbecke, K., Klett, G., and Rechenberg, B.: Wasserbeschaffenheit der wichtigsten Seen in der Bundesrepublik Deutschland: Datensammlung 1981-2000, 36/2003, 8 pp., 2003.

Woollings, T., Hannachi, A., and Hoskins, B.: Variability of the North Atlantic eddy-driven jet stream, Q.J.R. Meteorol. Soc., 136, 856–868, doi:10.1002/qj.625, 2010.

Wündsch, M., Haberzettl, T., Meadows, M. E., Kirsten, K. L., Kasper, T., Baade, J., Daut, G., Stoner, J. S., and Mäusbacher, R.: The impact of changing reservoir effects on the ^{14}C chronology of a Holocene sediment record from South Africa, Quaternary Geochronology, 36, 148–160, doi:10.1016/j.quageo.2016.08.011, 2016.

Yang, D. and Bowen, G. J.: Integrating plant wax abundance and isotopes for paleo-vegetation and paleoclimate reconstructions: a multi-source mixing model using a Bayesian framework, Clim. Past, 18, 2181–2210, doi:10.5194/cp-18-2181-2022, 2022.

Zahrer, J., Dreibrodt, S., and Brauer, A.: Evidence of the North Atlantic Oscillation in varve composition and diatom assemblages from recent, annually laminated sediments of Lake Belau, northern Germany, J Paleolimnol, 50, 231–244, doi:10.1007/s10933-013-9717-7, 2013.

Zech, M., Zech, R., Rozanski, K., Gleixner, G., and Zech, W.: Do n-alkane biomarkers in soils/sediments reflect the δ^2H isotopic composition of precipitation? A case study from Mt. Kilimanjaro and implications for paleoaltimetry and paleoclimate research, Isotopes in environmental and health studies, 51, 508–524, doi:10.1080/10256016.2015.1058790, 2015.

Figures
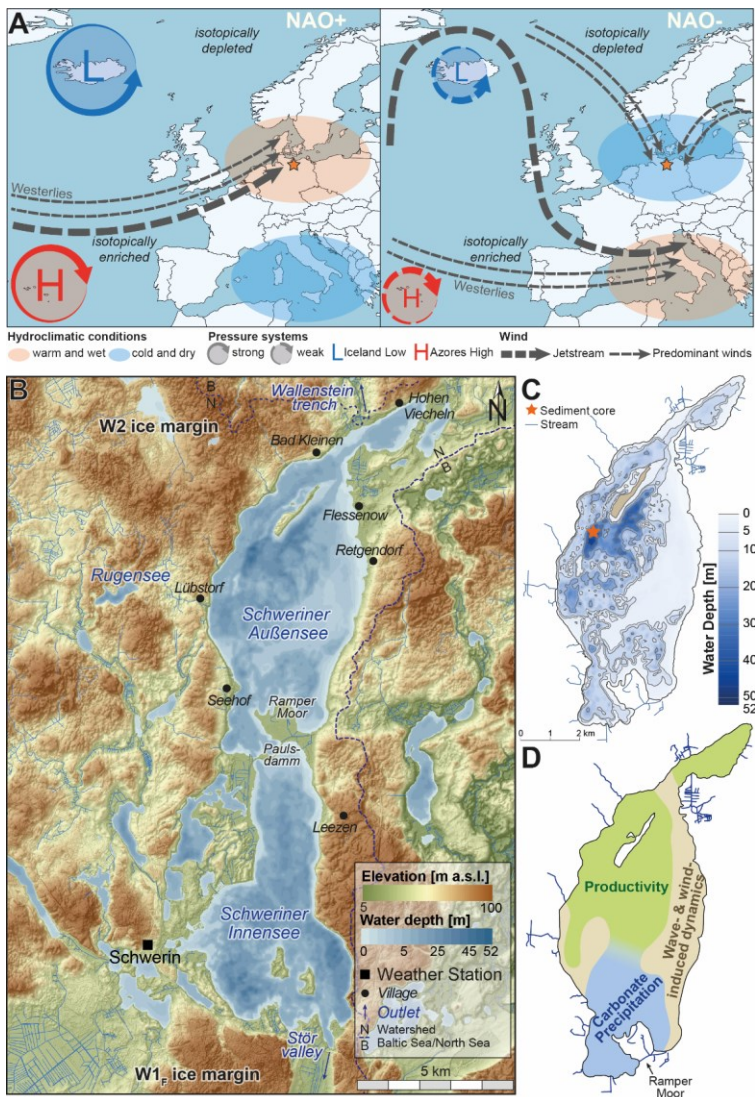
1355

Fig. 1: A) Conceptual overview of the North Atlantic Oscillation (NAO) illustrating the sea-level surface pressure during positive (NAO+, left) und negative (NAO-, right) phases and how these changes affect Westerlies and predominant winds at the study site of Schweriner See (orange star). B) Digital elevation model of the area surrounding Schweriner See including bathymetry and Weichselian moraines (W1F and W2) surrounding Schweriner See in the north and south. The outlets Wallensteingraben and Stör are indicated in the north and south. The semi-artificial Paulsdamm separates Schweriner See in two similar in size basins, Schweriner Außensee (north) and Schweriner Innensee (south). Although separated, water exchange is still possible (Wöbbecke et al., 2003). Also indicated is the Baltic Sea (B) / North Sea (N) water shed along the eastern and northern shoreline. C) Detailed bathymetric ~~M~~map of Schweriner ~~See~~ Außen~~S~~see including the coring position (orange star). D) Generalized classification of Schweriner ~~See~~ Außensee based on previous investigations on surface sediment samples by Adolph et al. (2023). The eastern, shallow water area is characterized by wave- and wind-induced dynamics (beige). The southern and northern parts are dominated by carbonate precipitation due to increased carbonate-rich groundwater inflow (blue) and productivity (green).
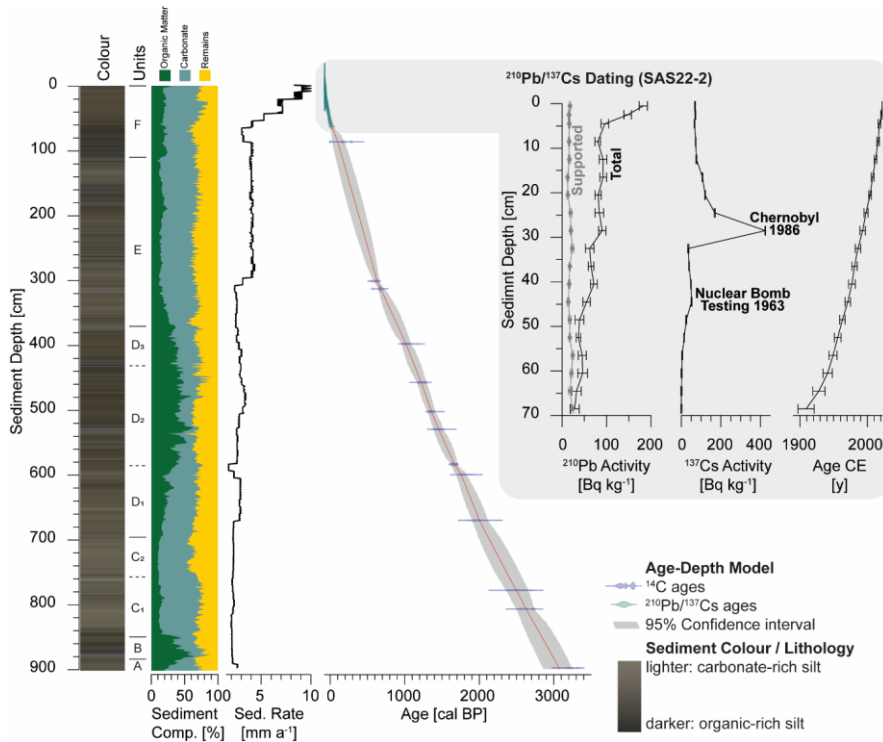
Fig. 2: Lithology and sediment colour of the composite record SAS21 (left). A higher organic content causes a darker colour, while a lighter colour is caused by increased carbonate precipitation. The sediment composition is shown as organic matter (=LOI$_{550}$; green), carbonates (= determined by Scheibler method; blue) and ~~residues~~ remains (yellow). The age-depth model is based on ^{14}C- (probability density function of the 2σ distribution, blue) and ^{210}Pb/^{137}Cs ages (teal). The mean age and the 95 % confidence interval are shown (centre). ^{210}Pb/^{137}Cs results show a distinct peak for the Chernobyl accident of 1986 (right).
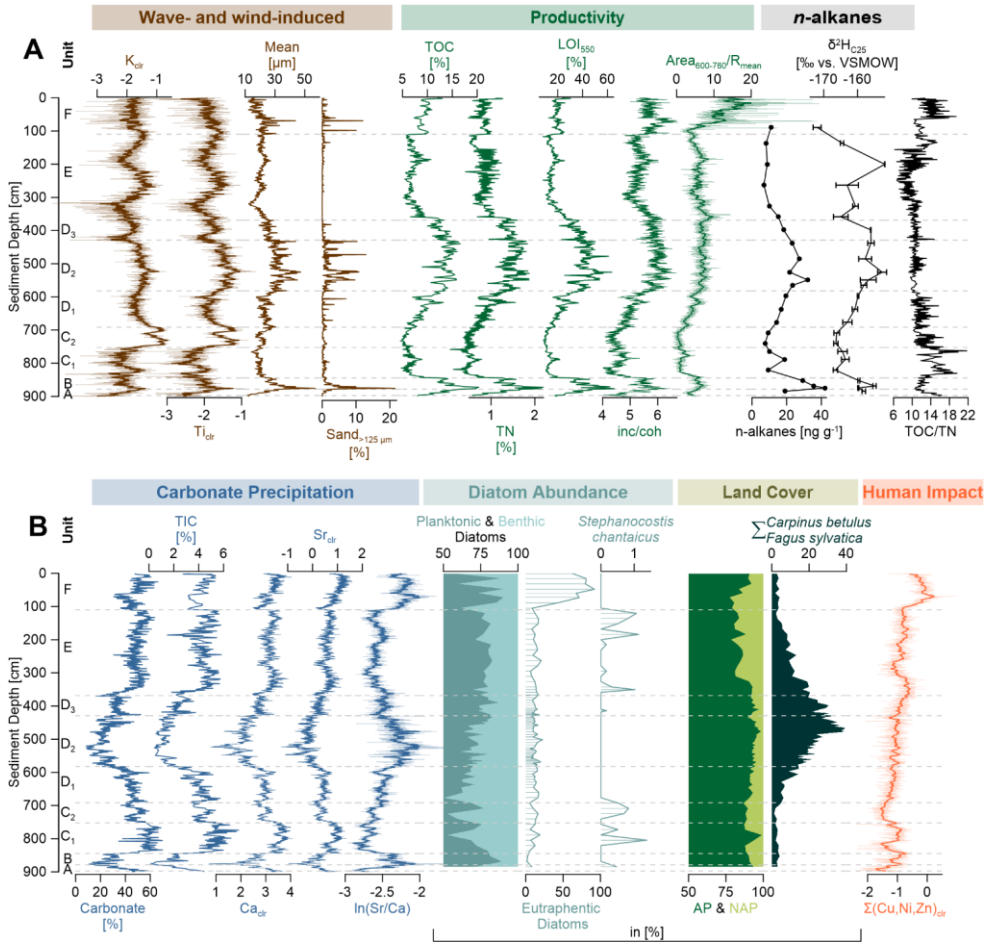
Fig. 3: Sedimentological, geochemical, spectral and micropaleontological characteristics of sediment sequence SAS21. A) Wave- and wind-induced processes (brown lines) are represented by potassium (K$_{clr}$), titanium (Ti$_{clr}$), grain size ~~M~~mean ~~and n,~~ ~~S~~sand fraction >125μm ~~63–125μm, Potassium (Sand~~K$_{>125μm}$~~) and Titanium (Ti$_{clr}$) Iron (Fe$_{clr}$) cannot be assigned to wave- and wind-induced processes or productivity.~~ Productivity (green lines) is shown by Total Organic Carbon (TOC), Total Nitrogen (TN), Loss on ignition 550 °C (LOI$_{550}$), inc/coh ratio, as well as Chlorophyll-a and its derivates (Area$_{600-760}$/R$_{mean}$, 101pt running average). The *n*-alkanes and their isotopic signatures are exemplary (δ^{2}H of *n*C$_{25}$). B) Carbonate precipitation (blue lines) is represented by the ~~c~~Carbonate content, Total Inorganic Carbon (TIC), Calcium (Ca$_{clr}$), Strontium (Sr$_{clr}$) and the Sr/Ca ratio. Diatom abundance is represented by the percentage of planktonic (teal area) and benthic (light blue area) diatoms, the abundance of eutraphentic diatoms indicating eutrophication and the under-ice blooming diatom *Stephanocostis chantaicus*. Land cover changes are indicated by palynological

investigations ~~and~~ represented by the ~~AP~~arboreal pollen (AP) and non-arboreal pollen~~/NAP~~ (NAP) (dark green vs. lime green area) ~~ratio~~ and summed up *Carpinus betulus* and *Fagus sylvatica* (very dark green area) percentages. Human impact is represented by $\sum$(Cu, Ni, Zn) (orange line). XRF data (Ti, K, inc/coh, Ca, Sr, ln(Sr/Ca) and $\sum$(Cu, Ni, Zn) are shown in 2 mm resolution and as 9 pt running average.
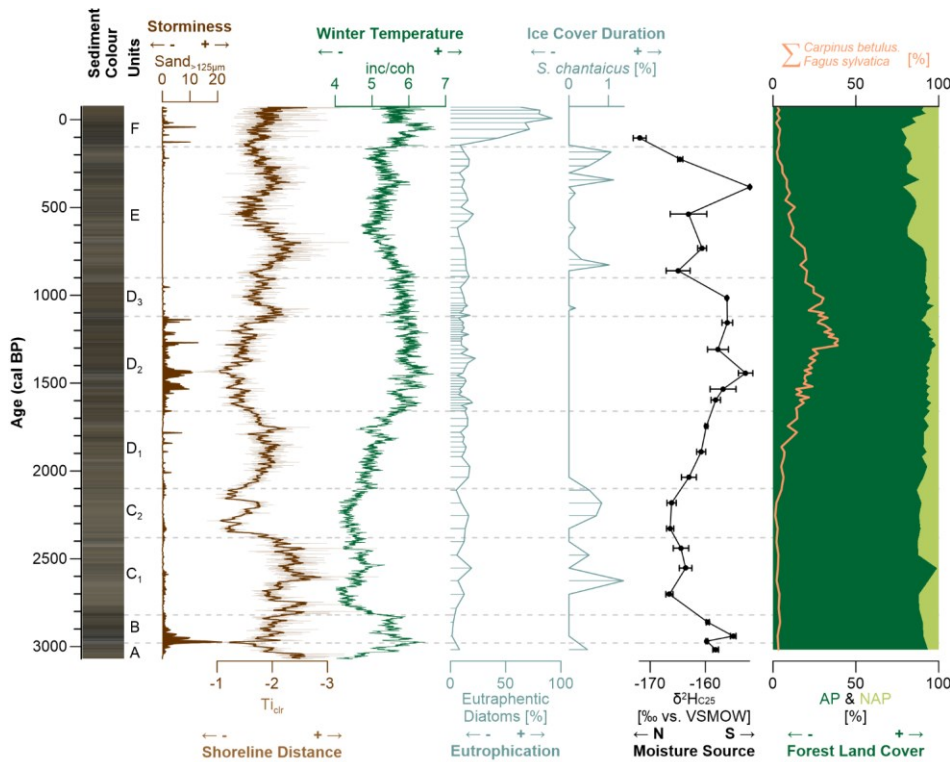
Fig. 4: Stratigraphic diagram of the past $3070^{+170}/_{-210}$ cal BP of SAS21 plotted on an age scale showing sediment colour as an indicator for lithological changes. Sand$_{>125\mu m}$ indicates changes in wave energy and, thus, storminess. Ti$_{clr}$ (9pt running average, brown line) indicates paleo-shoreline distance and inc/coh (green line) productivity, which is influenced by winter temperature variability. Eutraphentic diatoms represent the trophic state based on nutrient supply to Schweriner See, which only increases after $105^{+95}/_{-75}$ cal BP (unit F). The ~~d~~Diatom~~s~~ species *Stephanocostis chantaicus* (teal line) is strictly associated with ice cover duration (Scheffler and Padisák, 2000) and occurs in phases of low productivity. $\delta^2 H_{C25}$ indicates changes in the moisture source region. Land cover is shown by the relation between the arboreal pollen (AP) and non-arboreal pollen (NAP) ~~AP and NAP pollen~~ (dark green vs. light green area). Additionally, changes in the forest composition are represented by the sum of *Carpinus betulus* and *Fagus sylvatica* (orange line) indicating milder and moister conditions.
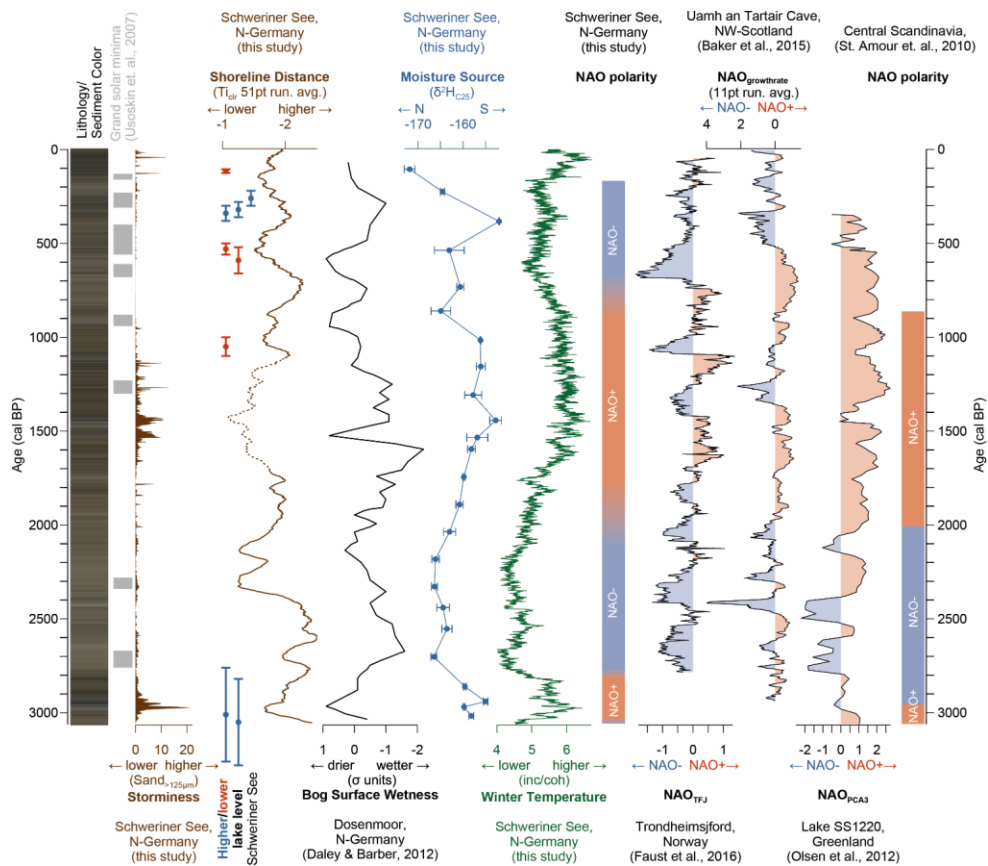
Fig. 5: Comparison of (hydro)climatic reconstruction from Schweriner See with different archives, ~~and~~ solar minima. (Usoskin et al., 2007) and storminess. Phases of higher/lower lake levels of Schweriner See inferred from (paleo)lacustrine landforms, archaeological findings and historical documents are shown in blue and red (Adolph et al., 2022; Lorenz et al., 2017; Konze, 2017; Umweltministerium Mecklenburg-Vorpommern, 2003) which agree with changes in shoreline distance (brown line, 51 pt average) inferred from Ti$_{clr}$ (this study) and hydroclimatic reconstructions from Dosenmoor (Daley and Barber, 2012) differentiating between drier and wetter conditions. Please note the reversed axis for both parameters. Moisture source region variations modulated by NAO variations are inferred from δ^2H_{C25}, with more ~~negative~~ depleted values suggesting a northwards displacement and/or a lower evaporative enrichment and, contrary, with more enriched values a southwards displacement and/or higher evaporative enrichment. These variations coincide with variations in winter temperature as inferred from productivity (~~normalized~~ inc/coh values, green line). ~~The~~ NAO ~~polarity~~ time slices ~~was~~ were inferred from distinct changes in δ^2H_{C25} and inc/coh. Hydroclimatic variations are compared to NAO reconstructions from Norway (Trondheimfjord = TJF, Faust et al., 2016), NW-Scotland (Stalagmite growthrate,

Baker et al., 2015), Greenland (PCA3 of PCA, Olsen et al., 2012) and Central Scandinavia (inferred lake water δ¹⁸O records of Lake Spåime and Lake Svartkalstjarn, St. Amour et al., 2010), showing a similar NAO variability over the last 3000 years.
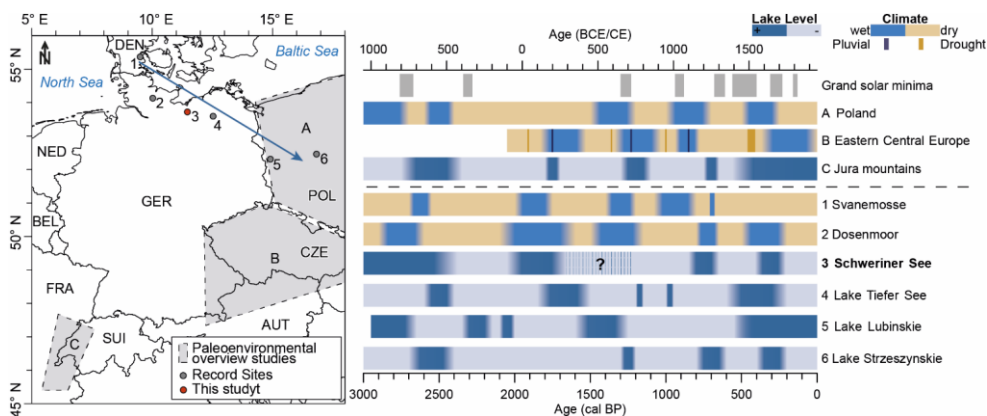
Fig. 6: Comparison of hydroclimate records covering the past 3000 years. Left: Map of the location of the records. Grey areas indicate the spatial extent of paleoenvironmental overview studies (A-C). The blue arrow indicates the NW-SE direction where the compared records are arranged. DEN: Denmark, POL: Poland, CZE: Czechia, AUT: Austria, SUI: Switzerland, FRA: France, BEL: Belgium, NED: Netherlands, GER: Germany. Right: Individual records are shown below the dashed line are and hydroclimatic overview studies above. Summarized records are from A1) Poland (Starkel et al., 2013), B2) Eastern Central Europe (Büntgen et al., 2021) and C3) Jura mountains (Magny, 2004). Hydroclimate reconstructions, which show wetter (blue bar) and drier (beige bar) conditions, are compared to lake-level variations and bog surface wetness reflecting hydroclimatic conditions differentiating between lower (light blue bars) and higher (dark blue bars) lake-levels from 14) Svanemosse (Barber et al., 2004), 25) Dosenmoor (Daley and Barber, 2012; Barber et al., 2004), 36) Schweriner See (this study), 47) Tiefer See (Theuerkauf et al., 2022), 85) Lake Lubińskie (Bonk et al., 2023) and 69) Lake Strzeszyński (Pleskot et al., 2018). Grand Ssolar minima are shown as suggested by Usoskin et al. (2007). The question marks and shaded area in the Schweriner See lake-level variations mark the period, masked by increased storminess. The lake level during the period was most likely higher.